AD-A069 564 POLYTECHNIC INST OF NEW YORK BROOKLYN DEPT OF MECHAN--ETC F/G 20/1
SOME NONLINEAR PROBLEMS IN TRANSONIC HELICOPTER ACOUSTICS.(U)
MAY 79 M P ISOM DAAG29-76-G-0035
UNCLASSIFIED POLY-M/AE-79-19 ARO-12937.1-E NL

1 OF 1
AD A069564

END
DATE FILMED
7 -79
DDC

Polytechnic Institute of New York, Brooklyn.

ARO 12937.1-E

(12)

LEVEL II

DEPARTMENT OF
MECHANICAL AND
AEROSPACE ENGINEERING

SOME NONLINEAR PROBLEMS IN TRANSONIC HELICOPTER ACOUSTICS

FINAL REPORT

BY

MORRIS P. ISOM

MAY 1979

U.S. ARMY RESEARCH OFFICE

GRANT DAAG29 76 G 0035

POLYTECHNIC INSTITUTE OF NEW YORK

POLY M/AE Report No. 79-19

Unclassified

SECURITY CLASSIFICATION OF THIS PAGE (When Data Entered)

REPORT DOCUMENTATION PAGE	READ INSTRUCTIONS BEFORE COMPLETING FORM
1. REPORT NUMBER	2. GOVT ACCESSION NO. 3. RECIPIENT'S CATALOG NUMBER
4. TITLE (and Subtitle) (6) SOME NONLINEAR PROBLEMS IN TRANSONIC HELICOPTER ACOUSTICS.	5. TYPE OF REPORT & PERIOD COVERED (9) Final rept.
	6. PERFORMING ORG. REPORT NUMBER
7. AUTHOR(s) (10) Morris P. Isom	8. CONTRACT OR GRANT NUMBER(s) (15) DAAG29-76-G-0035 new
9. PERFORMING ORGANIZATION NAME AND ADDRESS Polytechnic Institute of New York 333 Jay Street, Brooklyn, N. Y. 11201	10. PROGRAM ELEMENT, PROJECT, TASK AREA & WORK UNIT NUMBERS (12) 64 p.
11. CONTROLLING OFFICE NAME AND ADDRESS U. S. Army Research Office P. O. Box 12211 Research Triangle Park, NC 27709	12. REPORT DATE (11) May 1979 13. NUMBER OF PAGES 61
14. MONITORING AGENCY NAME & ADDRESS(if different from Controlling Office) (18) ARO (19) 12937.1-E	15. SECURITY CLASS. (of this report) Unclassified 15a. DECLASSIFICATION/DOWNGRADING SCHEDULE

16. DISTRIBUTION STATEMENT (of this Report)

Approved for public release; distribution unlimited.

(14) POLY-M/AE-79-19

17. DISTRIBUTION STATEMENT (of the abstract entered in Block 20, if different from Report)

18. SUPPLEMENTARY NOTES

The view, opinions, and/or findings contained in this report are those of the author(s) and should not be construed as an official Department of the Army position, policy, or decision, unless so designated by other documentation.

19. KEY WORDS (Continue on reverse side if necessary and identify by block number)

Acoustics, Helicopter, Nonlinear, Transonic

20. ABSTRACT (Continue on reverse side if necessary and identify by block number)

The nonlinear potential equation that determines the near aerodynamic and far acoustic fields of a hovering transonic helicopter blade is derived. Properties of this equation provide a qualitative description of characteristic surfaces associated with the nonlinear flow field.

A simple linearized acoustic formula is developed; a nonlinearization scheme is then applied to this formula, and the linear and nonlinear acoustic pressure profiles, including propagating acoustic shock waves, are numerically determined

→over

DD FORM 1 JAN 73 1473 EDITION OF 1 NOV 65 IS OBSOLETE

Unclassified 410139

SECURITY CLASSIFICATION OF THIS PAGE (When Data Entered)

20. and compared with experimental data.

A tentative conclusion is that the radiated sound field should become measurably different when the blade tip first punctures the sonic surface associated with the rotor differential equation. This conjecture is suggested by the mathematical properties of the rotor equation and recent experimental work.

SOME NONLINEAR PROBLEMS IN TRANSONIC HELICOPTER ACOUSTICS

Final Report

by

Morris P. Isom

May, 1979

U.S. ARMY RESEARCH OFFICE

GRANT DAAG29 76 G 0035

POLYTECHNIC INSTITUTE OF NEW YORK

POLY M/AE Report No. 79-19

THE FINDINGS IN THIS REPORT ARE NOT TO BE CONSTRUED AS AN OFFICIAL DEPARTMENT OF THE ARMY POSITION, UNLESS SO DESIGNATED BY OTHER AUTHORIZED DOCUMENTS.

TABLE OF CONTENTS

ABSTRACT

The nonlinear potential equation that determines the near aerodynamic and far acoustic fields of a hovering transonic helicopter blade is derived. Properties of this equation provide a qualitative description of characteristic surfaces associated with the nonlinear flow field.

A simple linearized acoustic formula is developed; a nonlinearization scheme is then applied to this formula, and the linear and nonlinear acoustic pressure profiles, including propagating acoustic shock waves, are numerically determined and compared with experimental data.

A tentative conclusion is that the radiated sound field should become measurably different when the blade tip first punctures the sonic surface associated with the rotor differential equation. This conjecture is suggested by the mathematical properties of the rotor equation and recent experimental work.

1. INTRODUCTION

It is now fairly well established that nonlinear effects play an important role in the propagation of sound generated by high speed helicopter blades. Calculations of rotor blade acoustic fields based on linear acoustic theory have been presented by several authors. Examples are the work of Farassat (ref. 1), Hawkings and Lowson (ref. 2), and Schmitz and Yu (ref. 3). These calculations are in good enough agreement to support the conclusion that linear theory does not adequately describe recent experimental data. In - flight experimental data of Vause, Schmitz, and Boxwell (ref. 4), and data taken in an anechoic facility designed for hovering rotor accoustic experiments (ref. 5) show wave form amplitudes that are 50 to 75% greater than amplitudes based on linear theory. The experimental data also show a distortion in wave form that cannot be accounted for by linear acoustics. An interesting feature of the data is that they show a wave profile that carries a pronounced acoustic shock wave into the far field. This far field discontinuity appears in the simplest experimental arrangement. For example, in reference 5, the model is a two-bladed rotor with rectangular planform , untapered in thickness, with aspect ratio 13.71 and NACA-0012 sections. The blade rotates in hover, and some runs have a thrust coefficient that is just large enough to keep the blade wakes out of the plane of rotation. The idea is to have the blade at near zero lift and then effectively to measure an in-plane acoustic profile that is caused almost entirely by blade thickness. The question is whether a linear theory of thickness sound predicts this measured profile ; the answer is apparently that it does not.

It is tempting to reach two conclusions here. Knowing that the experimentally determined acoustic profile carries a shock wave, and knowing the form of the profile provided by linear theory, the conclusions would be (1) that the experiments are displaying a wave form that is much like the profile found in sonic boom work, and (2) the linear theory may then be adjusted, using standard nonlinearization techniques, to give the propagating shock embedded in the distorted profile shown in the experimental data. Both conclusions are approximately correct. Clearly, the data show that disturbances of an aerodynamic nature on and near the blade surface, in its tip region, persist in a region off the blade tip in such a way that a wave forms; this wave propagates, rolls over, breaks, and forms a shock that moves off into the far field. It is also clear that in this picture there is an important distinction between flow events and pressure disturbances on and near the blade tip, and pressure disturbances at some distance (some few chords) from the blade tip. For contrast, consider a fixed wing of moderate aspect ratio, say 6, with rectangular planform and thickness ratio of about 0.1, that moves at constant velocity with zero lift at Mach number of around 0.9 or 0.95. It is well known that a region of embedded supersonic flow occurs next to a portion of the wing surface. Compression and expansion waves appear in this supersonic region that may be terminated by a shock wave. However, the wave system is trapped between the wing surface, the terminating shock wave, and a bubble-like sonic surface that forms over a part of the wing. No waves escape to infinity - there is no boom or bang. The conterpart of the fixed wing here is the rotor blade with larger aspect ratio - between 10 and 15 say, rectangular planform, thickness ratio around 0.1, and blade tip Mach number of 0.9 - 0.95. The blade may be in hover at zero

or near zero lift. Then the flow field near the blade surface, near the tip, is very similar to the field in the supersonic region of the fixed wing . The wing has constant free stream velocity, whereas the free stream velocity of the blade varies linearly along the span, increasing toward the tip. But otherwise a plot of pressure distribution on the rotor blade surface is quite similar to the distribution of the wing, and the location and strength of shocks on the two surfaces are also quite similar. The two surfaces show similar aerodynamic flow fields in their embedded supersonic regions. It is for this reason that it is convenient to classify the fluid dynamics near the high speed rotor tip as nonlinear and aerodynamic in nature, as opposed to acoustic.

The similarities described above appear in experimental data, and also in numerical calculations based on the small disturbance transonic potential flow equation. Examples of transonic near field calculations appear in two papers by Caradonna and Isom (refs. 6, 7).

Any similarity between the fixed wing and rotor blade problems disappears when the two far fields are examined. Pressure disturbances of the transonic ($M < 1$) fixed wing show a relatively rapid aerodynamic, nonacoustic decay, as they must if no sound is produced, while disturbances from the rotor blade show a slower, acoustic decay (the linear theory gives the usual R^{-1} geometric attenuation of a wave profile; nonlinear theory gives a somewhat faster decay). The distribution in the far fields is taken up in Section 2, where the complete small disturbance differential equation for a hovering rotor blade is derived. This rotor differential equation neatly summarizes the kinds of nonlinearities that affect the flow. The equation displays one nonlinearity that is effective

near the blade surface. Its only role is in the near field aerodynamics. One can see by inspection of the equation that this nonlinearity becomes weak and relatively unimportant far from the blade. In addition, the rotor equation shows a second nonlinearity that does not appear in subsonic fixed wing work. This second nonlinearity is not effective on the blade surface - it seems to have nothing to do with aerodynamics; its near field ineffectiveness is easily shown by scaling arguments. This nonlinearity decays with distance from the blade more slowly than does the aerodynamic one. It is finally the effect that maintains distortion and a shock wave in the pressure profile. It is the acoustic nonlinearity. However, a mere inspection of the differential equation does not show the extent of overlap - in some region off but near the blade tip - of the two nonlinear effects . Experimental data (ref. 8) suggest that a shock provided by aerodynamic effects on the blade surface merges , somewhere off the tip, with the more distinctively acoustic shock, the latter discontinuity then propagating off into the far field. Apparently we do not have a simple boom problem. It is probably not sufficient first to determine the linear acoustics of the rotor, and then to adjust the linear result with the usual nonlinearization schemes. Near field effects seem to spoil this simple program. Nevertheless, it is this kind of calculation that is taken up in Sections 3 and 4. The recommended alternative approach would be a full scale numerical attack on the nonlinear differential equation itself. Results from the latter kind of calculation are not yet available.

We first put linear theory in a very compact form using transonic scaling arguments and approximations. There is nothing arbitrary about these initial approximations - they could be improved if improvement were

required. The results of Section 3 are used to find and plot the linear wave profile. We then have an F-function on which to base a nonlinear acoustic calculation which is taken up in Section 4. The relevant methods here are all contained in Whitham's book (ref. 9). The linear calculation gives an amplitude that is too small in comparison with experimental data, and this profile cannot distort as it propagates. The calculation of Section 4 gives a distortion that has the correct qualitative appearance, and the nonlinearization provides the acoustic shock wave in the advancing profile. The adjusted linear theory cannot give a shock that begins on the blade surface, as experiment requires. At the end of Section 4 we modify the nonlinearization scheme in a way that is not entirely justified. It is noted that linear theory gives disturbance pressure proportional to thickness ratio δ to the first power, whereas transonic small disturbance theory gives disturbance pressure proportional to thickness ratio to the two-thirds power. We then simply rescale the linear pressure profile to make it proportional to $\delta^{2/3}$. This modification affects the amplitude of the wave, the distance from the blade tip at which a shock wave first appears, and the amount of distortion in the profile. Rescaling gives an amplitude that is larger than the linear amplitude by a factor $\delta^{-1/3}$ (which means larger by a factor of 2 for a 12% thick blade), and the shock moves in much closer to the blade. While these trends put the results in better agreement with experimental data, the method used to obtain them is not entirely satisfactory.

It may be worthwhile to comment on the methods used in this paper. There seem to be two quite different ways to approach the high speed helicopter acoustic problem. The first method would be based on the

Ffowcs Williams - Hawkings equation (ref. 10). The main thrust of most recent theoretical research in rotor acoustics has been based on some use or adaptation of this equation. In its most general form, it is a conversion of the equations of conservation of mass and momentum of fluid dynamics to a nonlinear scalar integral equation, with boundary conditions on the body surface accounted for. It is a generalization of Lighthill's equation, the equation that has been so useful in jet noise work. Our linear calculation of Section 3 is based on the linear term of the Ffowcs Williams - Hawkings equation (as are other linear calculations). Our final form of this linear term is unlike any other that has been used to study the rotor far field. It would be desirable to extract the essential nonlinear features of the FW-H equation and use them in this application. The main problem is that the Lighthill stress tensor or its derivatives must be integrated over all space exterior to the body surface. Convergence of this integral is very slow, and it is not yet clear how to approximate the stress tensor in a rational way, or how sensitive acoustic calculations are to approximations of this nonlinear term. This is not to say that the FW-H equation is unsuitable for the rotor problem. Indeed, it seems unlikely that better calculations can or should be entirely separated from this kind of method. The point is that the equation is still poorly understood in applications to nonlinear acoustic problems in infinite domains where wave profiles carry a shock wave. The equation has certainly not been fully exploited.

Alternatively, the aerodynamic and acoustic field of the rotor may be formulated in terms of the small disturbance, nonlinear partial differential equation for the velocity potential. This equation is discussed in Section 2. It seems likely that this equation will play an important role in the rotor acoustics area. Much is known about the numerical solution to

to small disturbance transonic potential equations in the fixed wing area. The rotor potential equation has a most unusual feature that distinguishes it from the fixed wing equation. There is a cylindrical region centered on the axis of rotation within which the flow is elliptic and where Dirichlet boundary condtions are applied on the blade surface. The equation becomes hyperbolic in the region exterior to the cylinder, and there radiation conditions must be imposed. The region outside the cylinder has real characteristics, and it is these characteristics that carry off disturbances from the blade to the far field. These characteristics from an envelope (always, for any non zero blade tip Mach number) and then a shock wave; it is the shock that has been experimentally measured. The differential equation is used in Section 4 to find corrections to the constant ambient sound speed in the far field, and then to improve the characteristics of the linear rotor potential equation. This procedure is called nonlinearization. It is now well known from sonic boom work.

2. THE EQUATION OF MOTION AND ITS NONLINEARITIES

The simplifying assumptions for flow over a transonic helicopter blade are essentially the same as those for transonic flow over a fixed wing: the gas has constant specific heats, any shock waves are weak and entropy jumps across them may be neglected, the disturbance velocity is irrotational and therefore has a potential, and only second order nonlinearities need be retained in the potential equation. With these assumptions the differential equation of motion is

$$\phi_{t't'} + \frac{\partial}{\partial t'}\left(\frac{u^2}{2}\right) + \vec{u} \cdot \nabla \phi_{t'} = a^2 \nabla^2 \phi. \tag{2.1}$$

The required approximation to the adiabatic sound speed squared is

$$a^2 = a_o^2 - (\gamma - 1)\phi_{t'}, \tag{2.2}$$

with a_o the sound speed in undisturbed air and $\vec{u} = \nabla \phi$. Equations (2.1) and (2.2) are correct for a coordinate system fixed in undisturbed air. We consider flow over a hovering helicopter blade; that is, flow over a blade that rotates at constant angular velocity $\vec{\omega}$ and that has no forward motion (zero advance ratio). Choose a system of cylindrical coordinates that rotates with the blade system and relative to which the blades are at rest. Let these coordinates be r, θ, z, with positive z pointing in the direction of the angular velocity vector $\vec{\omega}$ and perpendicular to the plane of rotation. Figure 1 shows a planview of two rectangular blades. The picture is simplified by ignoring the geometry of the blades near the rotor hub — there is no cut-out. Also shown are Cartesian coordinates x', y' fixed in undisturbed air, and coordinates x, y along the blade chord and blade span, and rotating with the blade. An observer at

point O in the plane of rotation has radial position r, polar angle θ' relative to the nonrotating y' axis, and angle θ relative to the rotating span axis y. The cylindrical coordinate systems are related by

$$r = r',$$
$$\theta = \theta' - \omega t',$$
$$z = z',$$

and the two time scales are the same, $t' = t$. The primed system is the inertial one, and the unprimed system is blade-fixed. The potential ϕ for a hovering rotor is a function only of the variables, r, $\theta' - \omega t$, and z. Time derivatives in (2.1) transform to

$$\phi_{t'} = -\vec{\omega} \times \vec{r} \cdot \nabla\phi = -\omega\phi_\theta, \quad \phi_{t't'} = \omega^2\phi_{\theta\theta}.$$

Using these results and some rearrangement of terms, equations (2.1) and (2.2) combine to give

$$\left[\omega^2 - \frac{a_o^2}{r^2} - (\gamma + 1)\frac{\omega}{r^2}\phi_\theta\right]\phi_{\theta\theta} - 2\omega\phi_r\phi_{r\theta} - 2\omega\phi_z\phi_{z\theta}$$

$$= \left[a_o^2 + (\gamma - 1)\omega\phi_\theta\right]\left(\phi_{rr} + \frac{\phi_r}{r} + \phi_{zz}\right). \qquad (2.3)$$

In all that follows, we need to consider only the flow over one blade of the two-bladed system. The reason is that a single blade has large aspect ratio, generally greater than 10, and the main concern is with flow events near a blade tip where the flow may be transonic. A good approximation is that flows near the two blade tips are essentially independent of each other. When we come to acoustic considerations, the

most intense part of the sound field is generated by a single tip, the one that is rotating toward an observer. We choose the blade on which $y \geq 0$.

Boundary conditions for (2. 3) are required. The main problems of rotor aerodynamics and acoustics are encountered with the simplest blade geometry: rectangular planform, no taper in thickness along the span, and constant section geometry. Figure 2 shows this simple geometry in blade fixed coordinates. A blade has chord ℓ and span L. We take the y-axis as the blade span axis running through section quarter chord points. The leading edge of the $y \geq 0$ blade is $x = -\ell/4$ and the trailing edge is at $x = 3\ell/4$. This disposition of coordinate axes is temporarily convenient. It will be more convenient later on to place the y-axis along the leading edge of the blade. We take blade section geometry to be

$$G(x, y, z) \equiv z - \delta \ell f\left(\frac{x}{\ell} + \frac{1}{4}\right) = 0, \qquad (0 \leq y \leq L)$$

where δ is the thickness ratio. Now let $\vec{V}$ be the velocity of air relative to the blade, so that

$$\vec{V} = -\vec{\omega} \times \vec{r} + \nabla\phi.$$

The condition of tangency at the blade surface is $\vec{V} \cdot \nabla G = 0$ on $G = 0$. A linearized boundary condition with the mean surface approximation is

$$\frac{\partial \phi}{\partial z} = \omega y \delta \dot{f} \qquad \text{on} \qquad z = 0, \tag{2. 4}$$

the dot over f indicating a derivative with respect to x/ℓ.

The behavior of a solution to equations (2. 3) and (2. 4) in the far field must be specified. The required behavior results from imposing a

radiation condition for $r \to \infty$. The form that this condition takes is most easily found by first transforming (2.3) to spherical coordinates R, α, θ. Let $\vec{R}$ be the position vector from the center of rotation to a variable point, with $|\vec{R}| = R$, α the angle that $\vec{R}$ makes with the positive z-axis, and θ the same in-plane polar angle as in Figure 1. Equation (2.3) in this coordinate system is

$$\left[\omega^2 - \frac{a_o^2}{R^2\sin^2\alpha} - (\gamma+1)\frac{\omega\phi_\theta}{R^2\sin^2\alpha}\right]\phi_{\theta\theta} - 2\omega\phi_R\phi_{R\theta} - 2\frac{\omega}{R^2}\phi_\alpha\phi_{\alpha\theta}$$

$$= \left[a_o^2 - (\gamma-1)\omega\phi_\theta\right]\left[\phi_{RR} + \frac{2}{R}\phi_R + \frac{1}{R^2\sin\alpha}\frac{\partial}{\partial\alpha}(\phi_\alpha\sin\alpha)\right]. \quad (2.5)$$

It is of interest to examine the form this equation takes for a linearized problem. Neglecting nonlinear terms in (2.5) gives the simple equation

$$\left(\omega^2 - \frac{a_o^2}{R^2\sin^2\alpha}\right)\phi_{\theta\theta} = a_o^2\left[\phi_{RR} + \frac{2}{R}\phi_R + \frac{1}{R^2\sin\alpha}\frac{\partial}{\partial\alpha}(\phi_\alpha\sin\alpha)\right]. \quad (2.6)$$

Equation (2.6) has the unusual property that it is <u>elliptic</u> for

$$\omega^2 < \frac{a_o^2}{R^2\sin^2\alpha}$$

and <u>hyperbolic</u> for

$$\omega^2 > \frac{a_o^2}{R^2\sin^2\alpha}.$$

In cylindrical coordinates, linearization of equations (2.3) gives elliptic behavior for

$$\omega^2 < \frac{a_o^2}{r^2},$$

and hyperbolic behavior for

$$\omega^2 > \frac{a_o^2}{r^2}.$$

The conclusion is that in linear theory there is a cylinder of radius $r = a_o/\omega$ inside which the flow is elliptic and outside which the flow is hyperbolic. We also conclude that no waves or wave propagation may appear inside this cylinder, while wave systems and wave propagation may occur outside it. The cylinder $r = a_o/\omega$ is called the sonic cylinder.

The tip Mach number M of a blade is defined as $M = \omega L/a_o$, where L is the blade radius. The sonic cylinder is then defined by

$$\frac{r}{L} = \frac{1}{M}.$$

The above comments refer to a linearized description of the flow, but it is evident that the main difficulties in calculating flow over a transonic rotor are intimately related to the fact that for M near one, the sonic cylinder lies very close to the blade tip. Referring to the nonlinear equation (2. 3), we will have elliptic and wave-free behavior for

$$\omega^2 - \frac{a_o^2}{r^2} - (\gamma + 1)\frac{\omega}{r^2}\phi_\theta < 0, \qquad (2.7a)$$

and hyperbolic and wave-like behavior for

$$\omega^2 - \frac{a_o^2}{r^2} - (\gamma + 1)\frac{\omega}{r^2}\phi_\theta > 0. \qquad (2.7b)$$

Of course ϕ_θ is not known a priori, and so the shape of the surface defined by setting the left-hand side of (2. 7) equal to zero is not known

until a solution is found. Nevertheless, we may conclude from (2. 7) that the sonic cylinder of linearized theory is replaced in a nonlinear theory by a kind of deformed cylindrical surface. If, for example, r and θ are held fixed while $z \to +\infty$ in (2. 7), then $\phi_\theta \to 0$ asymptotically, and the surface that separates elliptic from hyperbolic behavior returns (asymptotically) to the cylinder $r = a_o/\omega$. One may then say that the sonic surface defined by (2. 7) will depart from true cylindrical form in a region surrounding the blade tip, where the surface may have bulges toward or away from the blade tip. The surface defined by setting the left-hand sides of (2. 7) equal to zero is called the sonic surface.

It is tempting to make the following conjecture: Peak or high intensity sound generated by a transonic helicoptor blade first occurs when the blade tip penetrates the sonic surface. The idea is that the differential equation (2. 3) has a region of hyperbolic behavior in which there are real characteristics when the inequality (2. 7b) holds. Such a region exists for any non zero tip Mach number, no matter how small or large M may be. If M is very small, the space in which characteristics exist is at some great distance (roughly 1/M) from the center of rotation. The characteristics do not touch the blade surface. As $M \to 1$ from below, the sonic surface draws nearer to the blade tip. The farther this surface is from the tip, the more the shape is like a circular cylinder. The nearer the surface is to the tip, the more it will be deformed near the tip. There must then be some tip Mach number at which the sonic surface first comes in contact with the blade tip. If M is increased beyond this lower critical Mach number, a portion of the blade tip will protrude through the sonic surface. Real characteristics

on which disturbances propagate are then in contact with the blade surface, and these characteristics escape to infinity (i. e., to the far field).

There is as yet neither computational nor experimental evidence to support or disprove these qualitative remarks. Recent experimental work by Schmitz et al. (ref. 3) and the recent report by Yu et al. (ref. 8) suggest that our guess (conjecture) and the above remarks may be interesting.

We return to equation (2.6), the linearized potential equation in spherical coordinates. Let the meridian angle α be fixed and not zero, let $R \to \infty$, and neglect terms divided by R^2. Then (2.6) becomes

$$\omega^2 \phi_{\theta\theta} \doteq a_o^2 \left(\phi_{RR} + \frac{1}{R}\, \phi_R\right),$$

which is also

$$\omega^2 (R\phi)_{\theta\theta} = a_o^2 (R\phi)_{RR}. \tag{2.8}$$

This result shows simple behavior of solutions to (2.6) in the far field, for (2.8) is just a wave equation with solutions

$$R\phi = F_1(\omega R + a_o \theta) + F_2(\omega R - a_o \theta). \tag{2.9}$$

The characteristic surfaces of (2.8) are

$$\omega R + a_o \theta = c_1, \qquad \omega R - a_o \theta = c_2$$

where c_1 and c_2 are constants. The trace of these surfaces in the plane of rotation $z = 0$ are the Archimedean spirals

$$\omega r + a_o \theta = c_1, \qquad \omega r - a_o \theta = c_2 .$$

Only one of the functions F_1 and F_2 in (2.9) represents the solution ϕ for large R. The choice is based on the fact that small disturbances propagate in a "downstream" direction. For an observer fixed relative to the blade, the free streamlines are circles with centers on the axis of rotation. If the blade rotates in a counterclockwise direction relative to undisturbed air, then an observer fixed on the blade would see an undisturbed air motion in a clockwise direction, as in Figure 3. The figure shows arcs AB and AC of the traces in the plane $z = 0$ of the far field characteristics c_1 and c_2. The c_1 characteristic is the one that carries a disturbance at large R in the downstream direction from A to B. Hence F_1 is the proper choice and we have

$$R\phi \sim F(\omega R + a_o\theta, \alpha) \qquad (R \to \infty, \quad 0 < \alpha < \pi/2). \tag{2.10}$$

A subscript on F is no longer needed.

The linearized approximation (2.10) to the acoustic potential shows that wave propagation, in this approximation, is without distortion and subject only to geometric attenuation. This behavior is a result of assuming a constant speed of sound in the linear theory. A more accurate description of far field wave motion can be based on the linear result (2.10) with a nonlinear correction to the local sound speed. This technique results in a slightly faster than R^{-1} attenuation, produces distortion in the wave form F, and finally results in the formation of an acoustic shock wave. This method is applied and discussed in Section 4.

It is a fairly straightforward matter to nonlinearize the approximation (2.10) by correcting the far field sound speed. The main problem here is to find the right wave form F to nonlinearize. An F based

on the strictly linear theory is one candidate, but use of a linear F implies that the flow field near the blade surface is, in some sense, well approximated by a linear theory, and hence that nonlinear corrections are required only in the far field. This kind of problem — linear near field, nonlinear far field — often appears in the simplest sonic boom work. An unusual feature of the hovering rotor differential equation (2. 3) is that it has two kinds of nonlinearities. The first one appears in a region surrounding the blade tip. It is an aerodynamic nonlinearity and is associated with the transonic nature of flow in the blade tip region. If an observer point is near or in the plane of rotation, and the radial coordinate r is nearly equal to the blade radius L, then equation (2. 3) is well approximated by

$$\left[\omega^2 - \frac{a_o^2}{r^2} - (\gamma + 1)\frac{\omega}{r^2}\phi_\theta\right]\phi_{\theta\theta} = a_o^2(\phi_{rr} + \phi_{zz}). \qquad (2.11)$$

The problem posed by (2. 11) and the tangency condition is roughly similar to the nonlinear transonic problem for a fixed wing. However, any similarity between the fixed wing and rotor problems disappears in the far field. The far field rotor problem is best described by switching from the cylindrical equation (2. 3) to the corresponding spherical form (2. 5). In (2. 5), let $R \to \infty$ while the meridian angle α is fixed and not zero. Then (2. 5) reduces to

$$\omega^2\phi_{\theta\theta} - 2\omega\phi_R\phi_{R\theta} = \left[a_o^2 + (\gamma - 1)\omega\phi_\theta\right]\left(\phi_{RR} + \frac{2}{R}\phi_R\right). \qquad (2.12)$$

A slow variation of local sound speed for large R is embedded in this equation. The quadratic terms here are properly called acoustic nonlinearities. They are small perturbations to an otherwise linear

problem, as opposed to the nonlinearity in equation (2.11) which is not small relative to other terms in that equation.

This schematic division of the flow field into an inner aerodynamic tip solution and an outer acoustic field is not essential. In principle, a numerical solution could be based on the complete differential equation (2.3), with a surface tangency condition and an outer numerical boundary condition that simulates a radiation condition. Acoustic results from this kind of calculation are not yet available, although the near field aerodynamic problem has been explored by Caradonna and Isom (refs. 6 and 7).

The alternative course is to base the outer, nonlinear acoustic solution on the linear solution (2.10) and a corrected sound speed that is extracted from (2.12). This is essentially a sonic boom calculation. The simplest linear problem is the one that accounts for sound due to blade thickness alone. An explicit solution is available. In the following section we shall put that solution in its limiting transonic form. The result is a very compact formula that is suitable for a nonlinearization scheme that is required in an acoustic shock calculation.

3. LINEAR THEORY IN THE TRANSONIC LIMIT

The disturbance pressure p in the linear theory of potential flow over a rigid body is given by the well known formula

$$4\pi p = \rho_o \frac{\partial}{\partial t} \int \frac{v_n}{1 - M_R} \frac{dS}{\mathcal{R}}. \tag{3.1}$$

The symbols have their usual meaning. On the right-hand side, ρ_o is constant ambient density. If $\vec{v}$ is the velocity of a point on the body surface relative to stationary air, then v_n is the projection of $\vec{v}$ along the outward normal to the body surface; M_R is the radiation Mach number, and the script or fancy $\mathcal{R}$ is

$$\mathcal{R} = |\vec{R} - \vec{R}_o|, \tag{3.2}$$

where $\vec{R}$ is the observer's position vector and $\vec{R}_o$ is the position vector to an integration point on the body surface. The integral is over the body surface and all terms in the integrand are evaluated at retarded time τ. This time is defined by the retarded time equation

$$a_o(t - \tau) = \mathcal{R}, \tag{3.3}$$

where a_o is the constant ambient adiabatic sound speed.

For a hovering helicopter blade, it is convenient to consider the problem of determining p as defined in blade fixed coordinates. An observer fixed in undisturbed air would then appear to rotate relative to the blade in a clockwise motion about the blade center, if the blade motion is counterclockwise relative to stationary air. If we let $\vec{\eta} = (\eta_1, \eta_2, \eta_3)$ be Cartesian blade fixed coordinates, then $\vec{R}_o = \vec{R}_o(\vec{\eta})$ in (3.2) and the observer position vector in (3.2) is a function of retarded

time τ, so we have

$$\mathcal{R} = |\vec{R}(\tau) - \vec{R}_o(\vec{\eta})|.$$

The unit radiation vector $\hat{R}$ is defined as

$$\hat{R} = \frac{|\vec{R}(\tau) - \vec{R}_o(\vec{\eta})|}{\mathcal{R}} . \tag{3.4}$$

In the far field, as $|\vec{R}| \to \infty$, this vector is denoted by $\hat{r}$ instead of $\hat{R}$:

$$\hat{r} = \frac{\vec{R}(\tau)}{R} . \tag{3.5}$$

Let $\hat{i}$, $\hat{j}$, $\hat{k}$ be unit vectors along the η_1, η_2, η_3 axes. Let θ' be a cylindrical polar angle in the plane of rotation, measured positive counterclockwise from a fixed axis, and let ψ be the angle that the observer position vector $\vec{R}$ makes with the plane of rotation so that $\vec{R} \cdot \hat{k} \geq 0$ for $0 \leq \psi \leq \pi/2$. Then $\hat{r}$ is

$$\hat{r} = -\hat{i} \cos\psi \sin(\theta' - \omega\tau) + \hat{j} \cos\psi \cos(\theta' - \omega\tau) + \hat{k} \sin\psi . \tag{3.6}$$

Notation is mixed here. The unit coordinate vectors in (3.6) are fixed relative to the blade, while θ' is the observer in-plane angle measured from a reference axis fixed in undisturbed air. The quantity $\theta' - \omega\tau$ is therefore the observer's retarded angle relative to the blade span axis (relative to the blade, the observer does the rotating).

In the far field, formula (3.1) for p becomes the formula for linearized acoustic pressure,

$$4\pi R p = \rho_o \frac{\partial}{\partial t} \int \frac{v_n}{1 - M_R} \, dS.$$

The Doppler factor $(1 - M_R)^{-1}$ appears so often that we will denote it

by a special symbol D:

$$D \equiv \frac{1}{1 - M_R}, \tag{3.7}$$

so that acoustic pressure p is

$$4\pi R p = \rho_o \frac{\partial}{\partial t} \int v_n D \, dS. \tag{3.8}$$

Now it is fairly easy to prove that the acoustic pressure p is

$$4\pi R p = \rho_o a_o \frac{\partial}{\partial t} \int \hat{r} \cdot \hat{n} D \, dS, \tag{3.9}$$

where $\hat{n}$ is the blade outward pointing unit normal vector. Formulas (3.8) and (3.9) are acoustically or radiatively identical. The proof of this equivalence is given by Isom in reference (11). The formula (3.9) is more convenient for our purposes than its equivalent and better known form (3.8).

We now write out the integral (3.9) in more detail. The body is a blade with rectangular planform and constant section geometry, untapered in thickness. Let ℓ be the blade chord and L its span, the span being the distance from the center of rotation to the blade tip. Coordinate η_1 is along the chord, η_2 along the span axis, and η_3 is normal to the blade mean surface and points in the direction of $\vec{\omega}$. Section geometry is defined by

$$\eta_3 = \ell \delta f(\eta_1/\ell + b).$$

The nondimensional number b is the fraction of the chord from the blade leading edge to the blade span axis. This axis could be taken through the section quarter-chord points; however, its precise location does not play an important role in acoustic calculations; δ is the section thickness

ratio. Define nondimensional blade coordinates by

$$\zeta_1 = \frac{\eta_1}{\ell}, \quad \zeta_2 = \frac{\eta_2}{L}, \quad \zeta_3 = \frac{\eta_3}{\ell}.$$

Section geometry in these coordinates is

$$\zeta_3 = \delta f(\zeta_1 + b).$$

The unit vector $\hat{n}$ normal to the blade surface is then

$$\hat{n} = (\pm \hat{k} - \hat{i}\,\delta\,\dot{f})(1 + \delta^2\,\dot{f}^2)^{-1/2}.$$

The plus sign on $\hat{k}$ denotes the blade upper surface $\zeta_3 > 0$ and the minus sign the lower surface $\zeta_3 < 0$. The projection of the area element dS onto the blade mean surface is dS_o, with

$$dS = (1 + \delta^2\,\dot{f}^2)^{1/2}\, dS_o,$$

and

$$dS_o = d\eta_1\, d\eta_2 = \ell L\, d\zeta_1 d\zeta_2.$$

With these definitions, the formula (3.9) for acoustic pressure p is

$$4\pi R p = 2\rho_o a_o \ell L \frac{\partial}{\partial t} \int \left[\delta\,\dot{f}\cos\psi \sin(\theta' - \omega\tau) \pm \sin\psi\right] D\, d\zeta_1 d\zeta_2. \qquad (3.10)$$

A mean surface approximation has not yet been applied to the integrand of (3.10); the integrand in (3.10) is evaluated on the exact surface distribution and not on $\zeta_3 = 0$. We are, however, assuming a symmetrical section geometry, and the factor of two in (3.10) accounts for the upper and lower surfaces. Thus the integral need be taken only over the upper surface.

When the mean surface approximation is applied to (3.10), it is necessary to expand τ and the Doppler factor D as functions of the normal coordinate ζ_3. Both τ and D generally depend on ζ_1, ζ_2, and ζ_3, but we are here concerned only with the ζ_3 dependence, so the required expansions take the form

$$\tau(\zeta_3) = \tau(0) + \frac{\partial \tau(0)}{\partial \zeta_3} \delta f + \ldots \tag{3.11a}$$

$$D(\zeta_3) = D(0) + \frac{\partial D(0)}{\partial \zeta_3} \delta f + \ldots \tag{3.11b}$$

Function f appears on the right because ζ_3 is evaluated at $\zeta_3 = \delta f$, i.e., on the blade surface. It is tedious to apply the expansions (3.11) to the integrand of (3.10), but the process is straightforward. The result is

$$4\pi R p = \frac{2\rho_o a_o \ell L \delta}{\cos \psi} \frac{\partial}{\partial t} \int \dot{f} \sin(\theta' - \omega\tau) D \, d\zeta_1 d\zeta_2, \tag{3.12}$$

where now and henceforth it is understood that the integrand is evaluated on $\zeta_3 = 0$. The double integration is from blade leading edge to trailing edge and blade root $\zeta_2 = 0$ to blade tip $\zeta_2 = 1$.

We next introduce a transformation in (3.12) that will permit one integration by parts in the spanwise direction, thereby reducing the formula p to a single integral. The result will be that p is expressed as a single integral over the blade tip $\zeta_2 = 1$. The transformation proceeds as follows. It is well known that the gradient of retarded time τ with respect to dimensional coordinates η_1, η_2, η_3 is

$$\nabla_{\vec{\eta}} \tau = \frac{\hat{R}}{a_o} D .$$

Here $\hat{R}$ is the unit radiation vector defined in (3.4). In the far field $R \to \infty$ we write

$$\nabla_{\vec{\eta}} \tau = \frac{\hat{r}}{a_o} D ,$$

with $\hat{r}$ given by (3.5). The derivative of τ along the blade span axis ζ_2 is

$$\frac{\partial \tau}{\partial \eta_2} = \hat{j} \cdot \nabla_{\vec{\eta}} \tau = \hat{j} \cdot \hat{r} \frac{D}{a_o} = \cos\psi \cos(\theta' - \omega\tau) \frac{D}{a_o} .$$

We solve this equation for the Doppler factor D to get

$$D = \frac{a_o}{\cos\psi} \frac{1}{\cos(\theta' - \omega\tau)} \frac{\partial \tau}{\partial \eta_2} .$$

The formula (3.12) for p becomes

$$4\pi R p = \frac{\rho_o a_o^2 \ell L \delta}{\cos^2\psi} \frac{\partial}{\partial t} \int \dot{f} \tan(\theta' - \omega\tau) \frac{\partial \tau}{\partial \eta_2} d\zeta \, d\zeta_2 . \qquad (3.12a)$$

Substitute the identity

$$\frac{1}{\omega} \frac{\partial}{\partial \eta_2} \log |\cos(\theta' - \omega\tau)| = \tan(\theta' - \omega\tau) \frac{\partial \tau}{\partial \eta_2}$$

into (3.12a) to get

$$4\pi R p = \frac{\rho_o a_o^2 \ell \delta}{\omega \cos^2\psi} \frac{\partial}{\partial t} \int \dot{f} \frac{\partial}{\partial \zeta_2} \log|\cos(\theta' - \omega\tau)| d\zeta_1 \, d\zeta_2 .$$

The section slope distribution $\dot{f}$ depends only on ζ_1, so the ζ_2 integration may be carried out to give

$$4\pi R p = \frac{\rho_o a_o^2 \ell \delta}{\omega \cos^2\psi} \frac{\partial}{\partial t} \int \dot{f} \log \left| \frac{\cos(\theta' - \omega\tau_+)}{\cos(\theta' - \omega\tau_-)} \right| d\zeta_1 . \qquad (3.13)$$

Notation τ_+ means evaluate retarded time τ at chordwise points on the

blade tip section $\zeta_2 = 1$; τ_- means evaluate τ on chordwise points on the blade root section $\zeta_2 = 0$. The integral in (3.13) is from leading edge to trailing edge, on the tip and root sections.

Effective use of equation (3.13) requires some tailoring of the retarded time equation (3.3). In what follows, approximations are based on the assumption that the blade aspect ratio is large and the tip Mach number is near one. For a single rectangular blade with chord ℓ and span L, aspect ratio is L/ℓ. We define the small parameter ϵ as the

$$\epsilon = \ell/L .$$

Approximations in the retarded time equation will be based on the assumption that

$$\epsilon^{2/3} \ll 1 .$$

This approximation is analogous to the usual transonic fixed wing approximation that thickness ratio to the two-thirds power is small. The analogy results because here a transonic acoustic similarity parameter will appear that is based on $\epsilon^{2/3}$ rather than $\delta^{2/3}$.

We first note that peak or high intensity sound occurs in the far field when the quantity $\theta'-\omega\tau$ in equation (3.13) is near $\pi/2$. This result corresponds to the fact that an observer will measure peak sound when his line of sight is nearly perpendicular to the blade span axis, and the blade is rotating toward him. We therefore define a retarded angle ξ by

$$\theta'-\omega\tau = \pi/2 - \xi ,$$

where ξ will be small in a sense to be determined. The formula (3.13)

for p in terms of ξ is

$$4\pi Rp = \frac{2\rho_o a_o^2 \ell \delta}{\omega \cos^2 \psi} \frac{\partial}{\partial t} \int \dot{f} \log \left| \frac{\sin \xi_+}{\sin \xi_-} \right| d\zeta_1 . \tag{3.14}$$

The plus and minus signs on retarded angle ξ have the same significance as the subscripted signs on retarded time τ.

The retarded time equation (3.3) may be written

$$\omega t - \omega\tau = \frac{\omega}{a_o} (R^2 - 2\vec{R} \cdot \vec{R}_o + R_o^2)^{1/2} . \tag{3.15}$$

With R_o restricted to points on the blade surface and R large, the usual acoustic approximation to (3.15) is

$$\omega t - \omega\tau = \frac{\omega R}{a_o} - \frac{\omega}{a_o} \hat{r} \cdot \vec{R}_o . \tag{3.16}$$

Let $\vec{R}_o$ lie in the blade <u>mean</u> surface $\eta_3 = 0$. Then (3.16) is

$$\omega t - \omega\tau = \frac{\omega R}{a_o} + \frac{\omega}{a_o} \eta_1 \cos\psi \sin(\theta' - \omega\tau) - \frac{\omega}{a_o} \eta_2 \cos\psi \cos(\theta' - \omega\tau).$$

Nondimensionalize η_1 and η_2 by ℓ and L, use the definition $\epsilon = \ell/L$ and set $\theta' - \omega\tau = \pi/2 - \xi$ to get the <u>retarded angle equation</u>

$$\xi = \frac{\pi}{2} - \left(\theta' - \omega t + \frac{\omega R}{a_o}\right) - M\epsilon\, \zeta_1 \cos\psi \cos\xi + M\zeta_2 \cos\psi \sin\xi .$$

Take ξ to be small and note that the term in cos ξ is already of order ϵ, so that cos ξ may be set equal to one there. The term in sin ξ requires a two-term Taylor series approximation when M cos ψ is near one and the observer is in or near the plane of rotation. We then get an algebraic equation for ξ:

$$\xi = \frac{\pi}{2} - \left(\theta' - \omega t + \frac{\omega R}{a_o}\right) - M\epsilon\, \zeta_1 \cos\psi + M\zeta_2 \xi \cos\psi - \frac{M}{6} \zeta_2 \xi^3 \cos\psi .$$

Rearranging terms gives

$$\left(\frac{M}{6}\zeta_2 \cos\psi\right)\xi^3 + (1 - M\zeta_2 \cos\psi)\xi = \frac{\pi}{2} - \left(\theta' - \omega t + \frac{\omega R}{a_o}\right) - M \epsilon \zeta_1 \cos\psi. \tag{3.17}$$

The retarded angle ξ must be evaluated on the tip section where $\zeta_2 = 1$ and $\xi = \xi_+$, and at the root where $\zeta_2 = 0$ and $\xi = \xi_-$. The tip and root retarded angle equations are then

$$\left(\frac{M}{6} \cos\psi\right)\xi_+^3 + (1 - M \cos\psi)\xi_+ = \frac{\pi}{2} - \left(\theta' - \omega t + \frac{\omega R}{a_o}\right) - M \epsilon \zeta_1 \cos\psi, \tag{3.18}$$

$$\xi_- = \frac{\pi}{2} - \theta' - \omega t + \frac{\omega R}{a_o} - M \epsilon \zeta_1 \cos\psi. \tag{3.19}$$

The cubic term in ξ on the left of (3.18) is negligible when the tip Mach number M is small, or when the observer meridian angle ψ is near $\pi/2$, that is, when the observer is close to the axis of rotation. When either or both of these conditions hold, the entire blade surface becomes acoustically compact. On the other hand, when M is near one and the observer is in or near the plane of rotation so that the meridian angle ψ is near zero, the factor $1 - M \cos\psi$ that multiplies ξ in (3.18) becomes small and the cubic term is no longer relatively small. In this case, the outer portion of the blade surface is not acoustically compact. The presence of the cubic term reflects this noncompactness and the importance of time retardation. The simple equation for ξ_- results because acoustic source points near the center of rotation are always compact; sound from these low speed poinds has no significant Doppler shift.

The integral formula (3.14) requires

$$\frac{\sin \xi_+}{\sin \xi_-} \sim \frac{\xi_+}{\xi_-}, \tag{3.20}$$

only the first approximations to sin ξ for small ξ being needed here. The right-hand side of (3.20) is evaluated using (3.18) and (3.19) to give

$$\frac{\xi_+}{\xi_-} = \frac{1}{\left(\frac{M}{6} \cos \psi\right) \xi_+^2 + 1 - M \cos \psi} . \tag{3.21}$$

The final step in these approximations is to transonically scale the ξ_+ retarded angle equation (3.18). Define a scaled characteristic variable Ω by

$$\Omega \equiv \frac{\pi/2 - (\theta' - \omega t + \omega R/a_o)}{\epsilon M \cos \psi}, \tag{3.22}$$

and a scaled, retarded angle β by

$$\xi_+ \equiv \left[\frac{6(1 - M \cos \psi)}{M \cos \psi}\right]^{1/2} \beta .$$

With these definitions, the ξ_+ retarded angle equation (3.18) on the blade tip becomes

$$\beta^3 + \beta = \frac{1}{\sqrt{6}} \left[\frac{M \cos \psi}{1 - M \cos \psi}\right]^{3/2} \epsilon(\Omega - \zeta_1). \tag{3.23}$$

Finally, we define a transonic acoustic similarity parameter by

$$K \equiv \frac{1}{\sqrt{6}} \left[\frac{M \cos \psi}{1 - M \cos \psi}\right]^{3/2} \epsilon . \tag{3.24}$$

The scaled retarded angle equation (3.23) reduces to

$$\beta^3 + \beta = K(\Omega - \zeta_1). \tag{3.25}$$

If the similarity parameter K is small, then the entire rotor blade surface is acoustically compact. If K is O(1) or large, points on the blade surface are not compact and there is a significant variation of retarded angle (and time) over the surface.

Now replace the ratio ξ_+/ξ_- in equation (3.21) by

$$\frac{\xi_+}{\xi_-} = \frac{1}{1 - M\cos\psi} \quad \frac{1}{\beta^2 + 1} . \tag{3.26}$$

The right-hand side of (3.26) replaces $\sin\xi_+/\sin\xi_-$ in the integral formula (3.14) for p. Observe that when the logarithm of ξ_+/ξ_- is taken, the constant factor $(1 - M\cos\psi)^{-1}$ in (3.26) may be ignored because it gives zero contribution in the integral (3.14). This is because the leading and trailing edges of the blade lie in the plane of rotation, and the thickness distribution is zero at these two points.

The formula (3.14) for acoustic pressure is now

$$4\pi Rp = - \frac{2\rho_o a_o^2 \ell \delta}{\omega\cos^2\psi} \frac{\partial}{\partial t} \int \dot{f} \log(\beta^2 + 1)\, d\zeta_1 . \tag{3.27}$$

We next replace the t-derivative by a characteristic variable Ω-derivative, the $\Omega(t)$ relation being (3.22). Then (3.27) becomes

$$4\pi Rp = - 2\rho_o a_o^2 L \frac{\delta}{M\cos^3\psi} \frac{\partial}{\partial\Omega} \int \dot{f} \log(\beta^2 + 1) d\zeta_1 . \tag{3.28}$$

The slope distribution $\dot{f}$, with its singular behavior at a round leading edge, may be eliminated in favor of the thickness distribution f by an integration by parts. This requires

$$\frac{\partial\beta}{\partial\zeta_1} = - \frac{K}{3\beta^2 + 1}$$

from (3.25). Also, the Ω-derivative in (3.28) may be taken inside the integral. This requires

$$\frac{\partial \beta}{\partial \Omega} = \frac{K}{3\beta^2 + 1},$$

using (3.25) again. The last step is to move the origin of the integration variable ζ_1 to the blade leading edge. Let

$$\chi = \zeta_1 + b.$$

Our formula for acoustic pressure p is finally

$$p = -\frac{\rho_o a_o^2 L}{\pi R} \delta K^2 \int_0^1 f(\chi) \frac{\partial}{\partial \beta} \left[\frac{\beta}{(\beta^2+1)(3\beta^2+1)} \right] \frac{d\chi}{3\beta^2 + 1}, \qquad (3.29)$$

with the retarded angle β defined by

$$\beta^3 + \beta = K(\Omega + b - \chi). \qquad (3.30)$$

The nondimensional quantity b in (3.30) is the distance of the blade span axis from the blade leading edge. This distance is usually taken as $b = 1/4$.

It may be worthwhile to review what has been accomplished by the process of integration by parts, the large aspect ratio (small ϵ) approximation, and transonic scaling. The main points are:

(1) The integral formula (3.29) for p is only a <u>single</u> integral. Double integration over the entire planform has been avoided.

(2) The slope distribution $f(x)$ with its singular behavior at a round leading edge has been eliminated in favor of the thickness distribution $f(x)$ which is finite everywhere.

(3) The time derivative in front of the integral that represents p is taken inside the integral without introducing new singular behavior in the integrand.

(4) The function of retarded angle β that appears in the integrand of (3.29) is a regular function of β — it is not singular at any chordwise station χ.

(5) An acoustic similarity parameter K appears. The pressure p depends on ambient density, sound speed, and thickness ratio in a trivial way. The dependence of p on aspect ratio (or its inverse ϵ) and tip Mach number M when M is near one is entirely concentrated in K. This dependence is not so simple: p depends explicitly on K^2 in (3.29), and there is an implicit dependence on K through the dependence of the scaled retarded angle β on K.

(6) The form of an acoustic wave at a fixed, large radial position R is a function of the characteristic variable Ω defined by (3.22). This variable is also a characteristic variable of the linear partial differential equation that determines p. It was therefore clear from the beginning that the quantity Rp should depend on R, θ, and t through a variable like Ω. The form of this variable makes explicit the scale width of the wave profile. For example, if the observer is in the plane of rotation, then at a given (large) distance r and angular coordinate θ', the temporal duration of the wave — the time interval during which there is a significant, audible and measurable wave amplitude — is of the order of the parameter ϵM; or, for M near one, the width is the order ϵ, the inverse of the blade aspect ratio.

One must not place too much emphasis on any of the items listed above. Taken together, however, they produce a remarkably simple

formula for acoustic pressure. One advantage of the formula is that it is easy to use in a numerical calculation.

The formula (3.29) for p may be written in compact form as

$$p = \rho_o a_o^2 \frac{L}{R} F(\Omega), \tag{3.31}$$

where the nondimensional <u>profile</u> of an acoustic wave is

$$F(\Omega) \equiv -\frac{\delta K^2}{\pi} \int_0^1 f(\chi) \frac{\partial}{\partial \beta} \left[\frac{\beta}{(\beta^2+1)(3\beta^2+1)} \right] \frac{d\chi}{3\beta^2 + 1}. \tag{3.32}$$

The form (3.31) for p is especially convenient when nonlinear behavior and acoustic shocks are considered. One reason for getting the form (3.31), with the relatively simple form for $F(\Omega)$, is a reduction in the amount of numerical work required in a nonlinearization scheme. The function F would be identified in sonic boom work as a Whitham F-function.

4. ACOUSTIC SHOCKS

Acoustic pressure in the linear theory appears in Section 3 as

$$p = \rho_o a_o^2 \frac{L}{R} F(\Omega) \tag{4.1}$$

where the characteristic variable Ω is

$$\Omega = \frac{\omega t - \theta' - \omega R/a_o}{\epsilon M \cos \psi} \quad . \tag{4.2}$$

The profile of the wave is $F(\Omega)$, defined by equation (3.32). This profile remains undistorted with change in Ω, and the linear p is always shock free. It is known from experimental work (ref. 8) that sound waves generated by high speed rotors show a sharp, shock-like discontinuous form in the plane of rotation. These discontinuous wave forms occur even when the blade is operated at near zero lift, which suggests that the signal and its shape are caused by blade thickness and a slowly varying sound speed in the far field. Inspection of wave forms calculated from the simplest linear theory (as in Figure 4) immediately show that these forms will roll over and form a shock, and the shock may be calculated by correcting the far field sound speed. Whether the shock will have significant strenght (strong enough, for example, to rattle windows at some distance from the blade system) is not immediately evident from a graph such as Figure 4 .

Departure of the local sound speed from its ambient value a_o may be found from the nonlinear partial differential equation for the velocity potential. The asymptotic form of that equation at large distance from the blade surface is equation (2.12)

$$\omega^2 \phi_{\theta\theta} - 2\omega \phi_R \phi_{R\theta} = \left[a_o^2 + (\gamma - 1)\, \omega \phi_\theta \right] \left(\phi_{RR} + \frac{2}{R} \phi_R \right) . \quad (4.3)$$

Nonlinearization of the linear p of (4.1) proceeds by finding a correction to the constant sound speed a_o. This correction leads to improved characteristics for equation (4.3) that will replace the linear characteristic variable Ω.

Let a characteristic surface of equation (4.3) be denoted by $S(R, \theta) = 0$, and write S as

$$S = \theta + g(R) . \quad (4.4)$$

The surface $S = 0$ is a solution to the eikonal equation corresponding to (4.3),

$$\omega^2 S_\theta^2 - 2\omega \phi_R S_R S_\theta = \left[a_o^2 + (\gamma - 1)\phi_\theta \right] S_R^2 .$$

Replacing S by its form (4.4) gives an equation for $\dot{g}(R)$:

$$\omega^2 - 2\omega \phi_R g(R) = \left[a_o^2 + (\gamma - 1)\, \omega \phi_\theta \right] \dot{g}^2(R). \quad (4.5)$$

Treat ϕ_R and ϕ_θ in (4.5) as small and solve the quadratic equation for $\dot{g}$ to first order in these derivatives to get

$$\dot{g}(R) = \frac{\omega}{a_o} - \frac{\omega}{a_o^2} \phi_R - \frac{\omega^2}{a_o^3} \frac{\gamma - 1}{2} \phi_\theta . \quad (4.6)$$

The nonlinearization scheme replaces ϕ_R and ϕ_θ in (4.6) by their linear forms derived from equation (4.1). Pressure p and potential ϕ are related by

$$p = - \rho_o \phi_t ,$$

and so, using (4. 1) ,

$$\phi_t = - \frac{La_o^2}{R} F(\Omega) . \tag{4.7}$$

The derivative ϕ_t is also

$$\phi_t = \phi_\Omega \Omega_t = \frac{\omega}{\epsilon M \cos\psi} \phi_\Omega , \tag{4.8}$$

where (4. 2) has been used for Ω_t . Comparing (4. 7) and (4. 8) gives the important derivative

$$\phi_\Omega = - \frac{\epsilon M \cos\psi}{\omega} \frac{La_o^2}{R} F(\Omega) . \tag{4.9}$$

The derivatives ϕ_R and ϕ_θ that are needed in (4. 6) are calculated from (4. 9), retaining only radiative terms that are $O(R^{-1})$. We have

$$\phi_R = \phi_\Omega \Omega_R , \quad \phi_\theta = \phi_\Omega \Omega_\theta ,$$

and therefore

$$\phi_R = \frac{a_o L}{R} F(\Omega) , \quad \phi_\theta = \frac{a_o^2 L}{R} F(\Omega) .$$

Substituting these relations into (4. 6) for $\dot{g}$ gives

$$\dot{g}(R) = \frac{\omega}{a_o} - \frac{\omega L}{a_o} \frac{\gamma+1}{2} \frac{F(\Omega)}{R} \tag{4.10}$$

The essential approximation in nonlinearization is to treat Ω in equation (4. 10) as constant and then simply to integrate (4. 10) with respect to R. Doing so gives

$$g(R) = \frac{\omega R}{a_o} - \frac{\gamma+1}{2} M F(\Omega) \log \left(\frac{R}{R_o}\right) + c(\Omega) , \tag{4.11}$$

where c (Ω) is the constant of integration which, as indicated, may depend on Ω. The constant R_o in equation (4.11) is some radial position at which g(R) would take on its linear form $g(R) = \omega R/a_o + c(\Omega)$. The assumption is that there is some region relatively near the radiating body within which the acoustics may be treated in a linear fashion; this region is sufficiently close to the body so that waves have not propagated far enough to break, roll over, and form a shock wave. In the helicopter application, if the blade tip Mach number is sufficiently small, there will certainly exist a region of linear acoustics, and distortion in the profile will truly be limited to the far field. However, small tip Mach number generally implies small amplitude acoustics, and an acoustic shock may be so weak as not to merit the name shock wave. On the other hand, when tip Mach number is near one and the amplitude of an acoustic disturbance is relatively large, the acoustic wave may merge near the blade with an aerodynamic shock and the whole idea of some initial, near field, linear region that supports the far field acoustics may be lost. The experimental work of reference 8 suggests that the latter state of affairs may indeed be typical of a high speed rotor. The authors of reference 8 are continuing an experimental program in which the pressure field of a rotor is mapped in a continuous fashion from the blade surface to the far field.

The nonlinear program described here has deficiencies (which will be pointed out) but it should be kept in mind that a complete, thorough-going nonlinear calculation - near and far field - will certainly have embedded in its solution a nonlinear acoustics of the type that we are outlining. The crucial problem in a more accurate solution is to find the correct F (Ω) on which to base the far field solution.

Returning to equations (4.4) and (4.11), the characeristic surface S is

$$S = \theta + \frac{\omega R}{a_o} - \frac{\gamma+1}{2} MF(\Omega) \log\left(\frac{R}{R_o}\right) + c(\Omega) = 0. \qquad (4.12)$$

Recall that θ is the cylindrical angle in coordinates fixed to the blade. It is related to the inertial reference frame θ' and t by $\theta = \theta' - \omega t$. Setting $\theta = \theta' - \omega t$ in (4.12) and rearranging terms gives an expression for the improved Ω - characteristics

$$\omega t - \theta' - \frac{\omega R}{a_o} = -\frac{\gamma+1}{2} MF(\Omega) \log\left(\frac{R}{R_o}\right) + c(\Omega) . \qquad (4.13)$$

The correctly scaled characteristic variable Ω in the linear theory of Section 3 is

$$\frac{\omega t - \theta' - \omega R/a_o}{\epsilon M \cos\psi} = \Omega .$$

Dividing (4.13) by $\epsilon M \cos\psi$ and making an obvious choice for $c(\Omega)$ gives

$$\frac{\omega t - \theta' - \omega R/a_o}{\epsilon M \cos\psi} = \Omega - \frac{\gamma+1}{2\epsilon \cos\psi} F(\Omega) \log\left(\frac{R}{L}\right) . \qquad (4.14)$$

The constant R_o in the argument of the logarithm in equation (4.13) has been replaced by the blade span L. The choice of a length scale with which to nondimensionalize the radial coordinate R in (4.13) is not obvious. Lengths that are or are not suitable are based on the following observations:

1. The acoustic pressure is an <u>outer</u> solution to the flow about the blade. The blade surface has three characteristic and disparate length scales: the blade span L, blade chord ℓ, and section thickness t, with $L >> \ell >> t$. It is a general result that the smallest length scales do not play a role in the outer solution (the smallest lengths are, so to

speak, lost from our distant view of the blade). The only characteristic geometric blade length to survive in the outer solution would be the span, so it might be used in (4.13).

2. A wave length based on the blade fundamental frequency $f = \omega/2\pi$ is not a suitable scale. The entire acoustic wave form will propagate past a fixed observer with repetition frequency f, but this frequency is not a typical frequency in the wave form itself. Referring to the definition of the variable Ω in equation (4.2) it is apparent that a reference frequency for the wave form is $\omega/\epsilon M$, or, for M near one, the blade fundamental frequency times the blade aspect ratio, which is of course much larger than ω. Most of the acoustic energy is lodged in frequencies near $\omega/\epsilon M$. These analytical remarks agree, incidentally, with experimental work: a significant part of high speed helicopter sound is high frequency sound. Now let λ be a wave length based on the blade fundamental frequency ω, and let λ' be a wave length based on the angular frequency $\omega' = \omega/\epsilon M$. Then

$$\lambda' = \epsilon M \lambda .$$

Noting that

$$\lambda = \frac{2\pi}{M} L ,$$

we have for a length scale in the far field

$$\lambda' = 2\pi \epsilon L .$$

Although ϵ is small, as a practical matter the quantity $2\pi\epsilon$ is not so small. For an aspect ratio of 13.71 (used in ref. (8) and in our calculations) we have $\lambda' = 0.46 L$, and the distinction between the far field scales λ' and L is not a serious one. The simplest choice here is L.

Now define a new variable T as

$$T = \frac{\omega t - \theta' - \omega R/a_o}{\epsilon M \cos\psi} \quad . \tag{4.15}$$

Equation (4.14) for the new characteristic variable Ω is

$$T = \Omega - \frac{\gamma+1}{2\epsilon M \cos\psi} F(\Omega) \log\left(\frac{R}{L}\right) \quad . \tag{4.16}$$

Acoustic pressure p in (4.1) is a function of Ω in linear theory and is the same function of Ω in the nonlinear theory. What is required is p as a function of T. It is therefore necessary to invert (4.16) to find $\Omega = \Omega(T, R)$ and substitute this result into F in (4.1). Equation (4.16) is transcendental, and so the $\Omega(T, R)$ inversion must be a numerical calculation. We then have two sets of results:

<u>Linear theory</u>

$$p = \rho_o a_o^2 \frac{L}{R} F(\Omega) \quad , \tag{4.17a}$$

$$T = \Omega \quad . \tag{4.17b}$$

<u>Nonlinear theory</u>

$$p = \rho_o a_o^2 \frac{L}{R} F(\Omega) \quad , \tag{4.18a}$$

$$T = \Omega - \frac{\gamma+1}{2\epsilon \cos\psi} F(\Omega) \log\left(\frac{R}{L}\right) \quad . \tag{4.18b}$$

A shock will form when the $T(\Omega)$ relation (4.18b) forms an envelope with respect to Ω. This envelope is found by differentiating (4.18b) with respect to Ω to give

$$1 = \frac{\gamma+1}{2\epsilon M \cos\psi} \dot{F}(\Omega) \log\left(\frac{R}{L}\right) .$$

The radial position R/L where the envelope first forms and the shock begins is determined by the value of Ω that makes $\dot{F}$ a maximum. Thus

$$\log\left(\frac{R}{L}\right)_{MIN} = \frac{2\epsilon \cos\psi}{\gamma+1} \frac{1}{[\dot{F}(\Omega)]_{MAX}} \quad . \tag{4.19}$$

A difficulty appears: the value of R/L predicted by (4.19) for a typical rotor and flight conditions is in poor agreement with experiment. Let us use numbers in (4.19) for which experimental data are available (ref. 8). Take as aspect ratio 13.71, so that $\epsilon = 0.073$. Set $\psi = 0$ for an in-plane observer, and use $\gamma = 1.4$ for air. Let the blade have rectangular planform with NACA-0012 sections. For a tip Mach number 0.92, the theory of Section 3 gives 0.0179 as the maximum value of $\dot{F}$. Equation (4.19) then gives $R/L = 30$ for the in-plane radius at which a shock begins. According to the work of reference 8, at these conditions a shock begins <u>on</u> the blade surface (the usual transonic aerodynamic shock, much as for a fixed wing), but it then continues off the blade tip and into the far field, <u>without interruption.</u> This shock configuration will appear at tip Mach numbers less than 0.92 for the specified blade geometry. This discrepancy between theory and experiment is probably due to nonlinear effects that occur on the blade surface near the tip, and which persist for some few chords off the tip where more distinctively acoustic effects will begin. The blade surface nonlinearities cannot, of course, be accounted for by a simple modification of linear theory.

The above mentioned inaccuracy in the nonlinearization may be partially remedied. The linear result has an acoustic pressure and an F-function that are proportional to blade thickness δ. It is known, however, that near the blade surface, the pressure distribution that is based on the nonlinear differential equation (2.11) in proportional to $\delta^{2/3}$, not δ. This is a transonic scale effect that appears in rotor theory, just as it does in fixed wing theory. We may then modify the F-function in equations (4.18) by dividing it by $\delta^{1/3}$, thereby making F proportional to $\delta^{2/3}$. The result is a

Modified nonlinear theory: $$p = \rho_o a_o^2 \frac{L}{R} \frac{F(\Omega)}{\delta^{1/3}} \qquad (4.20a)$$

$$T = \Omega - \frac{\gamma+1}{2\epsilon \cos\psi} \frac{F(\Omega)}{\delta^{1/3}} \log\left(\frac{R}{L}\right) . \qquad (4.20b)$$

Equation (4.18b) for the shock initial radius is changed to

$$\log\left(\frac{R}{L}\right)_{MIN} = \frac{2\epsilon \cos\psi}{\gamma+1} \frac{\delta^{1/3}}{[\dot{F}(\Omega)]_{MAX}} . \qquad (4.21)$$

This rescaling of the F-function is not entirely arbitrary. An exact solution to the differential equation (2.3) would yield the entire flow field, both aerodynamic and acoustic. In the far field, an approximation to that solution would take the form (4.20), and the approximation would be a good one. The F-function that approximates the exact solution would not, however, be the linear F used in (4.20); it would be some other F that approximates the far field behavior to the numerical solution to the differential equation . (We leave aside here the fact that if an exact solution to the differential equation were known, then a boom approximation to that solution would not be necessary ; but this is not to say that such an approximation would be of no interest). The numerically derived F would have the scaling that goes with the differential equation. Nevertheless, it has to be acknowledged that merely rescaling the nonlinearized formula (4.18) to fit a known property of an exact solution is something of an ad hoc adjustment.

Let us find the initial, in-plane location of the shock from the modified formula (4.20), using the same data that were used in the unmodified formula (4.18) : aspect ratio = 13.71, M = 0.92, rectangular planform, NACA-0012 sections. Then (4.21) gives R/L = 5, as opposed

previous $R/L = 30$. Movement of the shock toward the tip is a desirable trend in view of the results of reference 8. The boom formulas should, of course, be applied in the region $R/L >> 1$. Their application here is treading into the region $R/L = 5$, which scarcely qualifies as very large.

The remaining acoustic shock calculations of this report are based on the modified scheme (4.20). A discussion of numerical results based on this and the previous section is taken up in Secion 5.

5. NUMERICAL RESULTS AND CONCLUSIONS

Numerical results shown in Figures 4-10 are presented as plots of acoustic pressure against a characteristic variable at some fixed in-plane radius. Since the radius is fixed, the characteristic variable may be considered a scaled time variable. Linear calculations are based on equation 4.17 ; the characteristic dependent variable is Ω , defined by equation (4. 2). Nonlinear p is calculated using (4. 20a) with a characteristic dependent variable T defined by (4.20b). In the linear theory, Ω and T are identical; in a nonlinear calculation, Ω is eliminated in favor of T , the functional relation being equation (4. 20b).

Some of the blade geometry is fixed in Figures 4-10: planform is rectangular, there is no twist or taper in thickness, thickness ratio is 12% , aspect ratio is 13.71. All calculations are for hover. Tip Mach number is 0. 92 and pressure is calculated in the plane of rotation. Two blade sections are used, biconvex and NACA-0012. Geometry and flight conditions were selected for comparison with experimental data of reference 8.

It is not necessary to recapitulate here the well known results of elementary sonic boom theory on which our nonlinear results are based. The method and elaborations on it appear in Whitham's book. It is enough to note that the system (4. 18) or (4. 20) lead to wave form distortion and finally to wave breaking and shock formation. Location of a shock, when one occurs, and calculation of portions of the wave profile separated by the shock wave are found by the usual methods.

Two features that are currently used in an initial comparison of theoretical results with experimental data are the peak negative pressure and the general shape of the pressure distribution as a function of time,

or as a function of some equivalent time variable (here our Ω or T).

A completely linear calculation for a blade with biconvex sections is shown in Figure 4. The graph is symmetrical about $\Omega = 0$ because the span axis of the blade is taken to be the section half-chord point for biconvex profiles; the span axis is therefore an axis of symmetry of the blade. Figure 5 shows a linear calculation for a blade with NACA-0012 sections. Flight conditions for Figures 4 and 5 are the same. Figure 5 also has a symmetrical appearance, but here the axis of symmetry goes through a value of Ω slightly greater than zero. This is because the span axis of the 0012 blade was taken as the section quarter-chord point, as it would be for a blade in actual flight conditions.

A surprising result is that apart from the location of axes of symmetry, Figures 4 and 5 are nearly identical. The peak negative pressure in both cases is $-481\,N/m^2$. According to reference 5, the measured peak negative pressure in approximately $-960\,N/m^2$ for a 1/7 scale model of the UH-1H helicopter blade at the flight conditions of Figure 5. The measured peak is therefore larger in magnitude than the linear result by very nearly a factor of 2. This discrepancy seems to be typical of all linear calculations.

A characteristic of Figures 4 and 5 that affects harmonic content is the temporal scale width of the pressure profile. We define this width to be the time interval that separates the two positive pressure peaks. The real time width Δt is related to the separation $\Delta\Omega$ of the peaks in Figures 4 and 5 by $\Delta t = (\epsilon\, M/\omega)\, \Delta\Omega$ (this follows from the definition of Ω in equation (4.2)) . The angular frequency ω may be determined from $\omega = (a_o/L)M$. For ambient sound speed $a_o = 341 m/s$ and a blade radius $L = 1.04$ m (the scale model radius of ref. 5), we have $\omega = 302$ rad/s at a tip Mach number of 0.92. The separation $\Delta\Omega$ in

Figures 4 and 5 is nearly 2. The real time width is therefore $\Delta t = 0.4$ milliseconds. The corresponding measured widths taken from reference 5 are 0.36 ms for M = 0.9, and 0.43 ms for M = 0.96. Our calculated value of 0.4 ms therefore agrees quite well with experiment.

Figures 6 and 7 show nonlinearized calculations for the biconvex and 0012 blades. There is one startling result in these figures: the peak negative pressure is $-975\ N/M^2$, and this number agrees almost precisely with the measured value of about $-960\ N/m^2$ in reference 5. This result must be accepted with some caution when we recall the particular kind of nonlinearization used to generate Figures 6 and 7. The usual, straightforward sonic boom nonlinearization has been modified, as already explained in Section 4, by rescaling the F-function to make it proportional to thickness ratio to the two-thirds power. This rescaling affects amplitude, location of a shock wave if one occurs, and the amount of distortion in the wave profile - it permeates the whole calculation. The modification is suggested by observing that pressure in the exact, nonlinear transonic theory is proportional to $\delta^{2/3}$ near the blade. The observation to make here is that agreement of calculated results in Figures 6 and 7 with experimental data may or may not be fortuitous. Calculations at other hover tip Mach numbers are not yet available for comparison with the full range of tip Mach number data of reference 5.

It will be noticed that Figures 6 and 7 are distorted versions of 4 and 5. The right-hand portions of 6 and 7 are steeper than the corresponding parts in 4 and 5. In fact, the right-hand portions of 6 and 7 are so steep as to suggest the appearance of a shock wave, but this is not the case for the data shown in the legends of the two figures.

Figure 8 is a graph of acoustic pressure for a biconvex blade, now calculated at the breaking radius $R/L = 3.25$. This radius is determined by equation (4.21). The steepest portions of Figures 8 and 9 are very steep indeed: casual inspection of these graphs might suggest that shocks occur here. Of course, a shock must appear in the pressure profile at any radius greater than the breaking radii of Figures 8 and 9.

Figure 10 is a wave profile for the biconvex blade, calculated at $R/L = 6.48$. A full-fledged shock wave now appears. The shock extends almost from the peak negative pressure to the peak positive pressure; the steepest part of the profile is almost all shock wave. The physical dimensions of the anechoic facility used to generate the data of reference 5 do not allow measurement at radial distances corresponding to Figure 10, when a 1 meter radius blade is used, so comparison with experiment cannot be made here.

The main conclusion to be drawn from Figures 4-10 is that a nonlinear method gives the distortion, and finally the shock wave, that brings calculated results closer to experimental data than does any linear theory. These results are a forceful reminder that good nonlinear technique, whether in the Ffowcs Williams-Hawkings equation or in the complete rotor differential equation, is essential if the full range of experimental data is to be accounted for.

Several qualitative conclusions emerge from a discussion of the nonlinear potential equation that governs the rotor near field aerodynamics and the far acoustic field. Two nonlinearities appear. The first one is effective near the blade surface and controls the local aerodynamics, including the shock wave that may occur on the blade;

it is not effective in the far field. The second nonlinearity is decisive in maintaining distortion and a shock wave in the propagating acoustic profile; it has no counterpart in fixed wing ($M < 1$) aerodynamics. Scaling arguments show this second nonlinearity to be unimportant on the blade surface.

The characteristic surfaces of the rotor differential equation may shed some light on recent experimental results. It has been observed that a hovering transonic blade has a kind of lower critical Mach number at which abrupt changes in the acoustic field appear. At and above this Mach number, the blade surface and the far field seem to become linked by an uninterrupted shock wave, and the sound field becomes measurably more intense. The appropriate conjecture is that this behavior is initiated when the extreme blade tip first touches or punctures the sonic surface defined by the nonlinear potential equation. The validity and usefulness of this idea will require numerical solution of the differential equation and more detailed experimental investigation.

6. NOTATION

a_o	Constant adiabatic sound speed = 341 m/s .
b	Distance of blade span axis from blade leading edge as a fraction of blade chord.
D	Doppler factor = $(1-M_R)^{-1}$.
f	Blade section thickness distribution; blade fundamental frequency.
$F(\Omega)$	Profile of acoustic wave.
$\hat{i}, \hat{j}, \hat{k}$	Unit vectors along x, y, z, or η_1 , η_2 , η_3 blade fixed axes.
$\hat{i}', \hat{j}', \hat{k}'$	Unit vectors along x', y', z' nonrotating axes.
K	Acoustic similarity parameter.
ℓ	Blade chord
L	Blade radius (span).
M	Blade tip Mach number.
M_R	Radiation Mach number.
p	Disturbance pressure; acoustic pressure.
r	Cylindrical radial distance; in-plane radial coordinate.
$\hat{r}$	Far field unit radiation vector.
R	Spherical radial distance.
$\mathcal{R}$	$\lvert \vec{R} - \vec{R}_o \rvert$.
$\vec{R}$	Observer position vector.
$\vec{R}_o$	Position vector of point on blade surface.
$\hat{R}$	Unit radiation vector.
S	S = O : Characteristic surface of rotor differential equation.
S_o	Projection of blade surface onto plane of rotation.
t	Time.
t'	Time (= t) .

T	Characteristic variable in nonlinear theory.
v_n	Projection of blade velocity along outward normal.
$\vec{V}$	Velocity of air relative to blade.
x, y, z	Blade-fixed axes.
x', x', z'	Nonrotating axes.
α	Observer spherical angle measured from axis of rotation.
β	Scaled retarded angle.
γ	Ratio of specific heats.
δ	Thickness ratio.
ϵ	Inverse of blade aspect ratio $\doteq \ell / L$.
$\zeta_1, \zeta_2, \zeta_3$	Nondimensional blade fixed coordinates.
η_1, η_2, η_3	Dimensional blade fixed coordinates.
θ	Cylindrical polar angle relative to span axis.
θ'	Cylindrical polar angle in nonrotating frame.
ξ	Retarded angle $= \pi/2 - (\theta' - \omega t')$.
ρ_o	Ambient density $= 1.23\ kg/m^3$.
τ	Retarded time .
ϕ	Velocity potential.
ψ	Observer meridian angle (out-of-plane angle) .
ω	Blade angular velocity.
$\vec{\omega}$	Blade angular velocity vector.
Ω	Scaled characteristic variable.

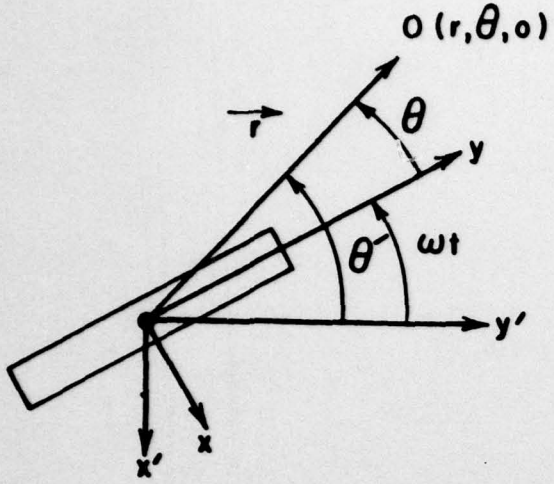

FIGURE 1

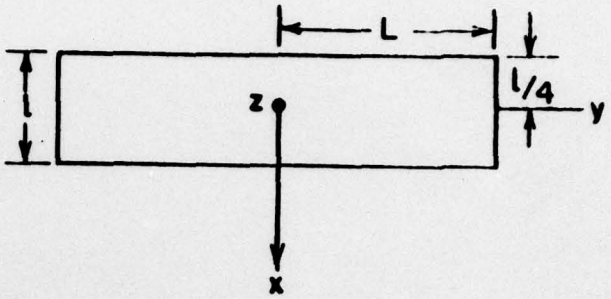

FIGURE 2

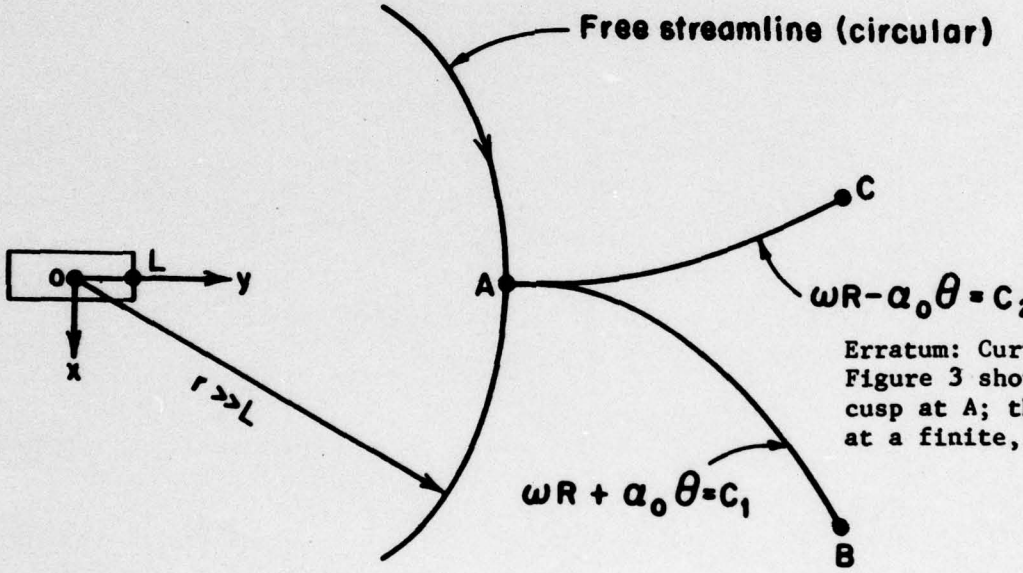

FIGURE 3

Erratum: Curves AB and BC in Figure 3 should not meet in a cusp at A; they should intersect at a finite, nonzero angle.

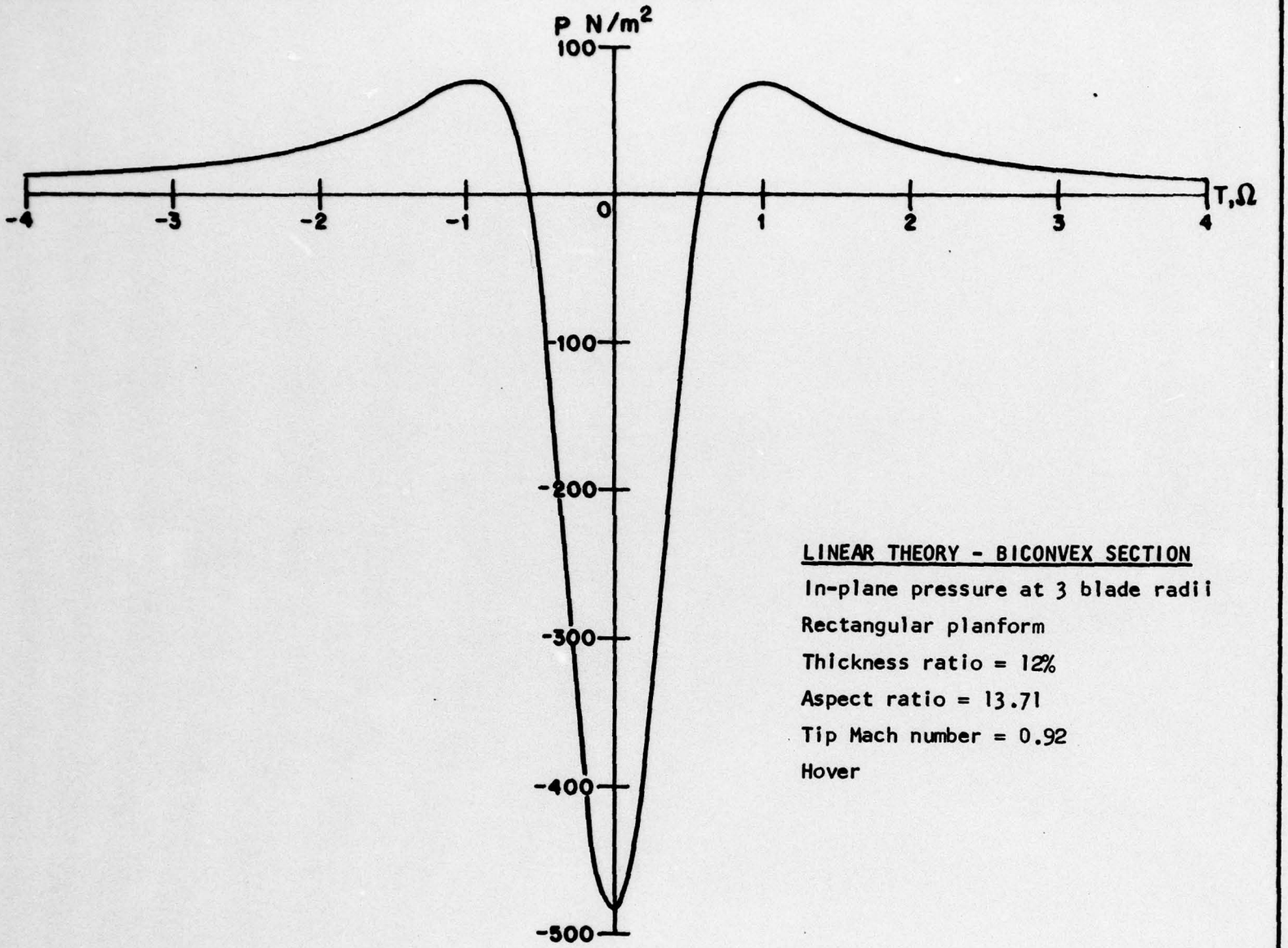

LINEAR THEORY - BICONVEX SECTION

In-plane pressure at 3 blade radii

Rectangular planform

Thickness ratio = 12%

Aspect ratio = 13.71

Tip Mach number = 0.92

Hover

FIGURE 4

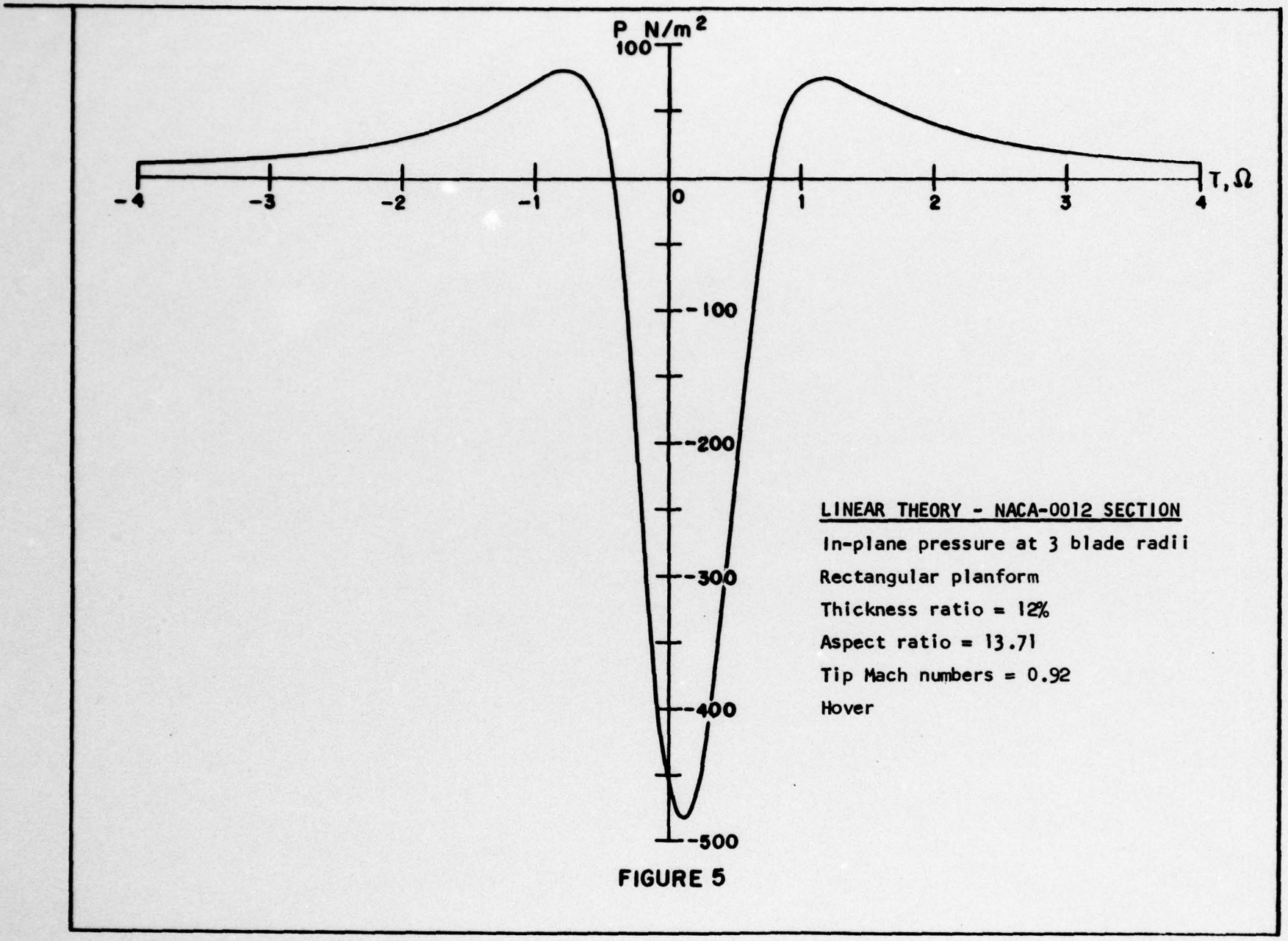
P N/m²
100
-100
-200
-300
-400
-500
-4
-3
-2
-1
0
1
2
3
4
T, Ω
LINEAR THEORY - NACA-0012 SECTION
In-plane pressure at 3 blade radii
Rectangular planform
Thickness ratio = 12%
Aspect ratio = 13.71
Tip Mach numbers = 0.92
Hover

FIGURE 5

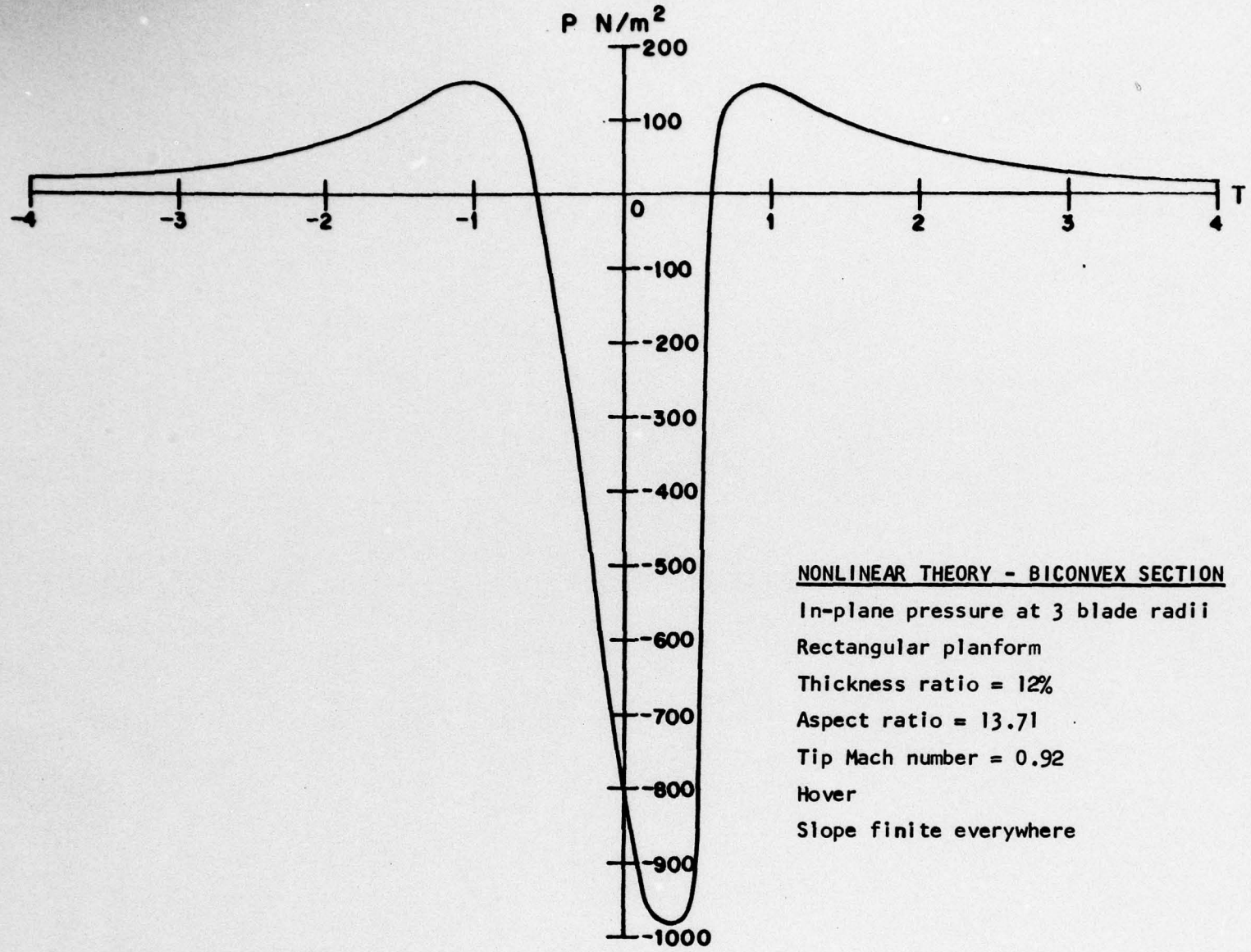

NONLINEAR THEORY - BICONVEX SECTION

In-plane pressure at 3 blade radii

Rectangular planform

Thickness ratio = 12%

Aspect ratio = 13.71

Tip Mach number = 0.92

Hover

Slope finite everywhere

FIGURE 6

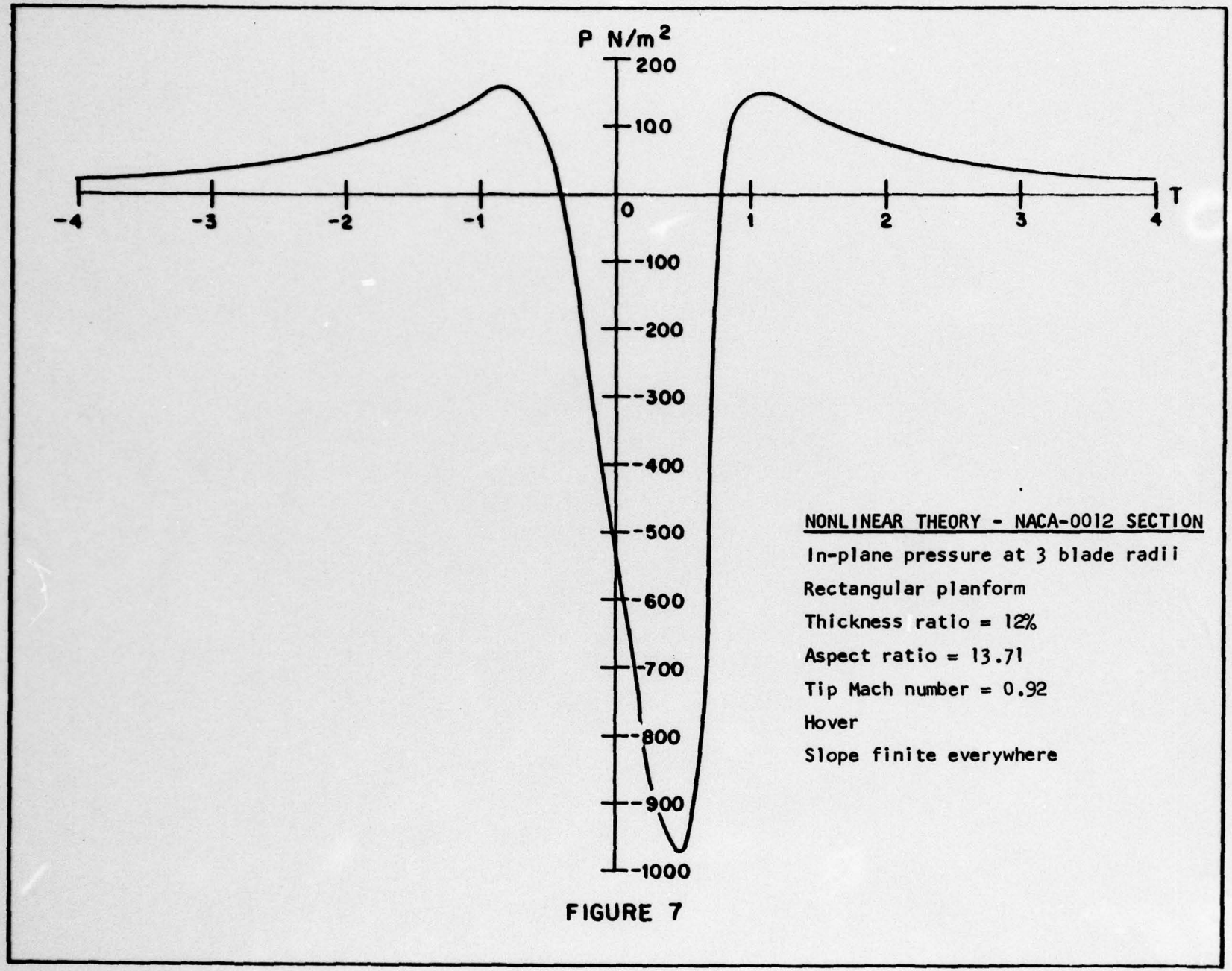
P N/m²
200
100
-100
-200
-300
-400
-500
-600
-700
-800
-900
-1000
-4
-3
-2
-1
0
1
2
3
4
T
NONLINEAR THEORY - NACA-0012 SECTION
In-plane pressure at 3 blade radii
Rectangular planform
Thickness ratio = 12%
Aspect ratio = 13.71
Tip Mach number = 0.92
Hover
Slope finite everywhere

FIGURE 7

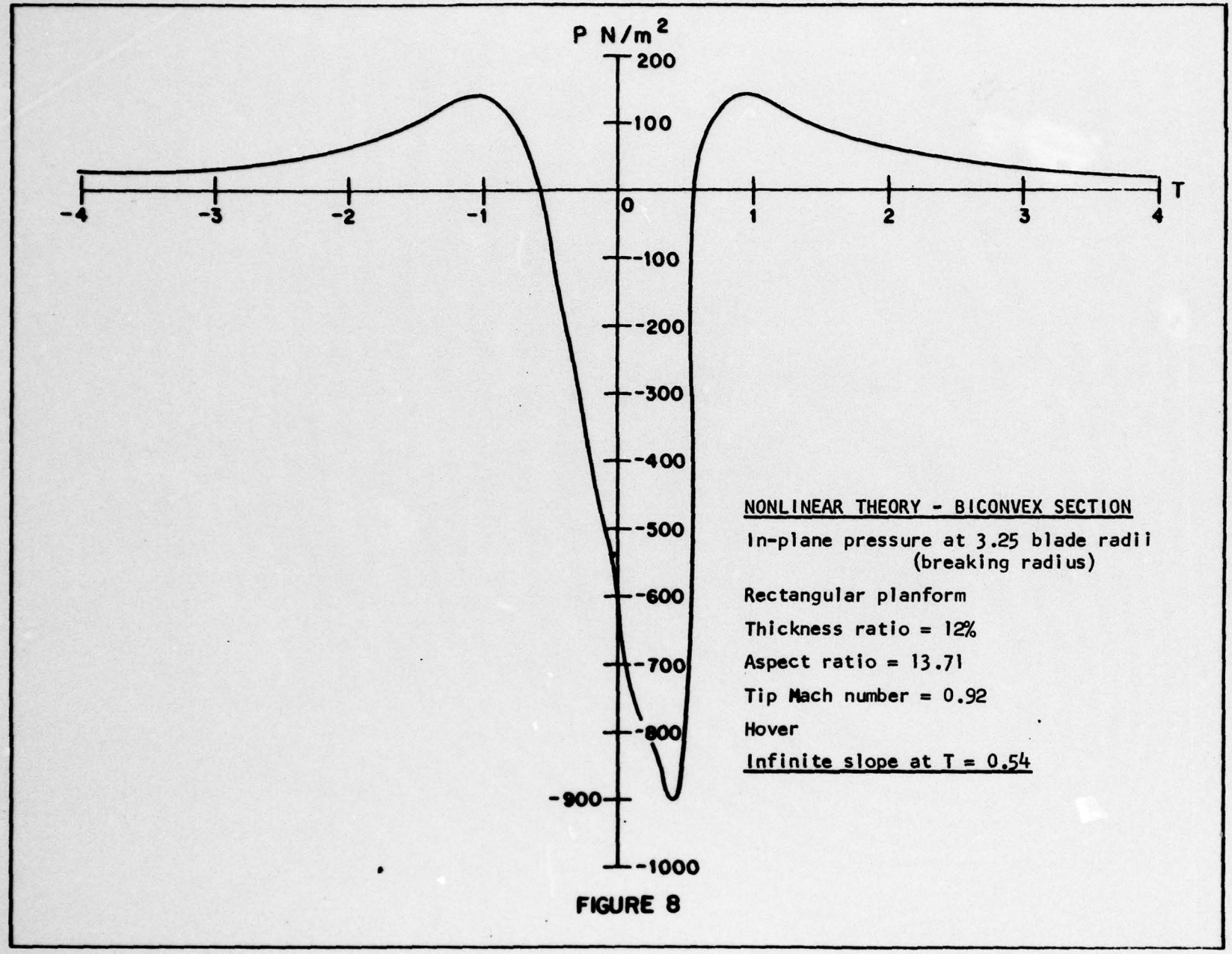
P N/m 2
200
100
-100
-200
-300
-400
-500
-600
-700
-800
-900
-1000
-4
-3
-2
-1
0
1
2
3
4
T
NONLINEAR THEORY - BICONVEX SECTION
In-plane pressure at 3.25 blade radii (breaking radius)
Rectangular planform
Thickness ratio = 12%
Aspect ratio = 13.71
Tip Mach number = 0.92
Hover
Infinite slope at T = 0.54

FIGURE 8

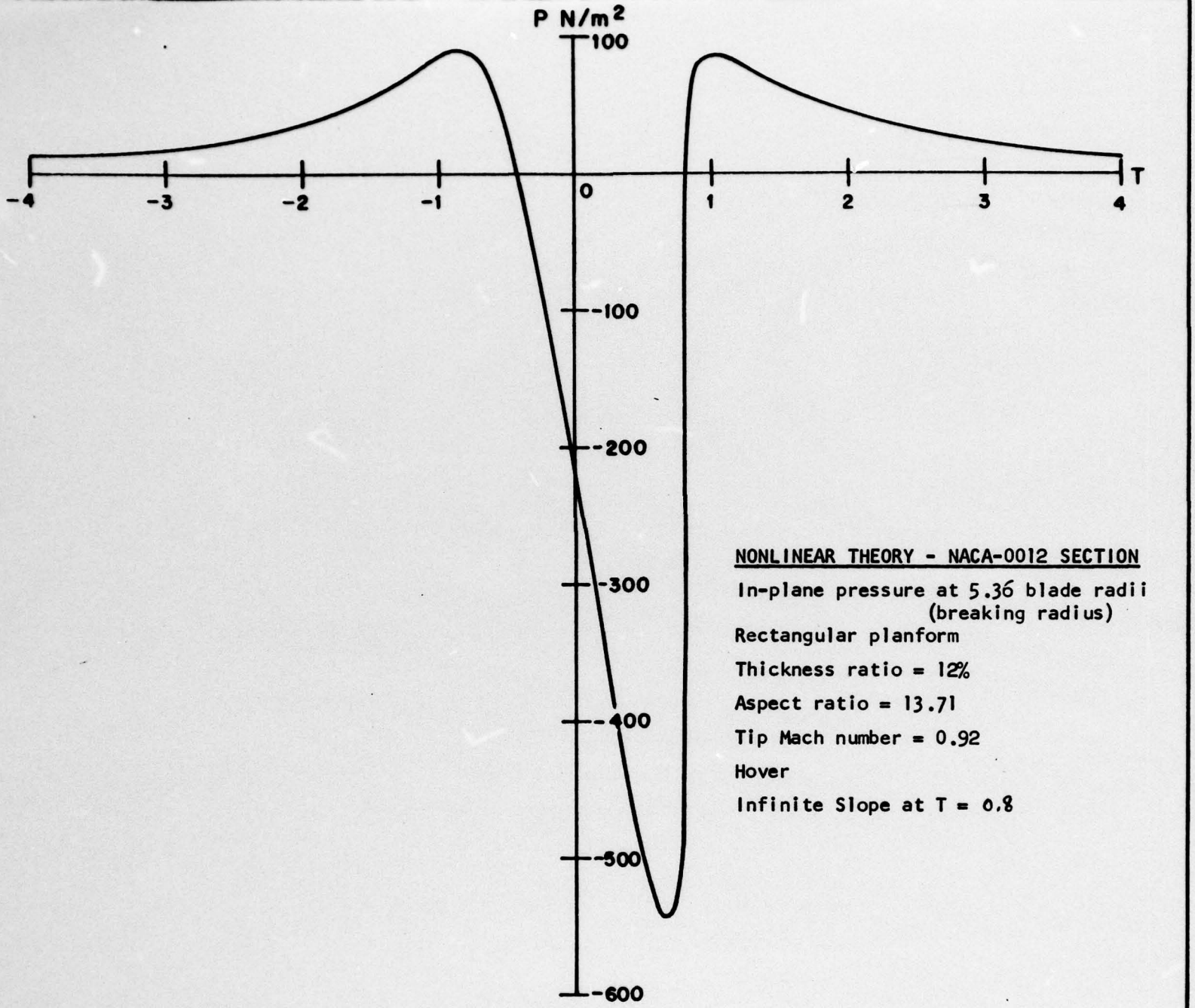
P N/m²
100
-100
-200
-300
-400
-500
-600
-4
-3
-2
-1
0
1
2
3
4
T
NONLINEAR THEORY - NACA-0012 SECTION
In-plane pressure at 5.36 blade radii
(breaking radius)
Rectangular planform
Thickness ratio = 12%
Aspect ratio = 13.71
Tip Mach number = 0.92
Hover
Infinite Slope at T = 0.8

FIGURE 9

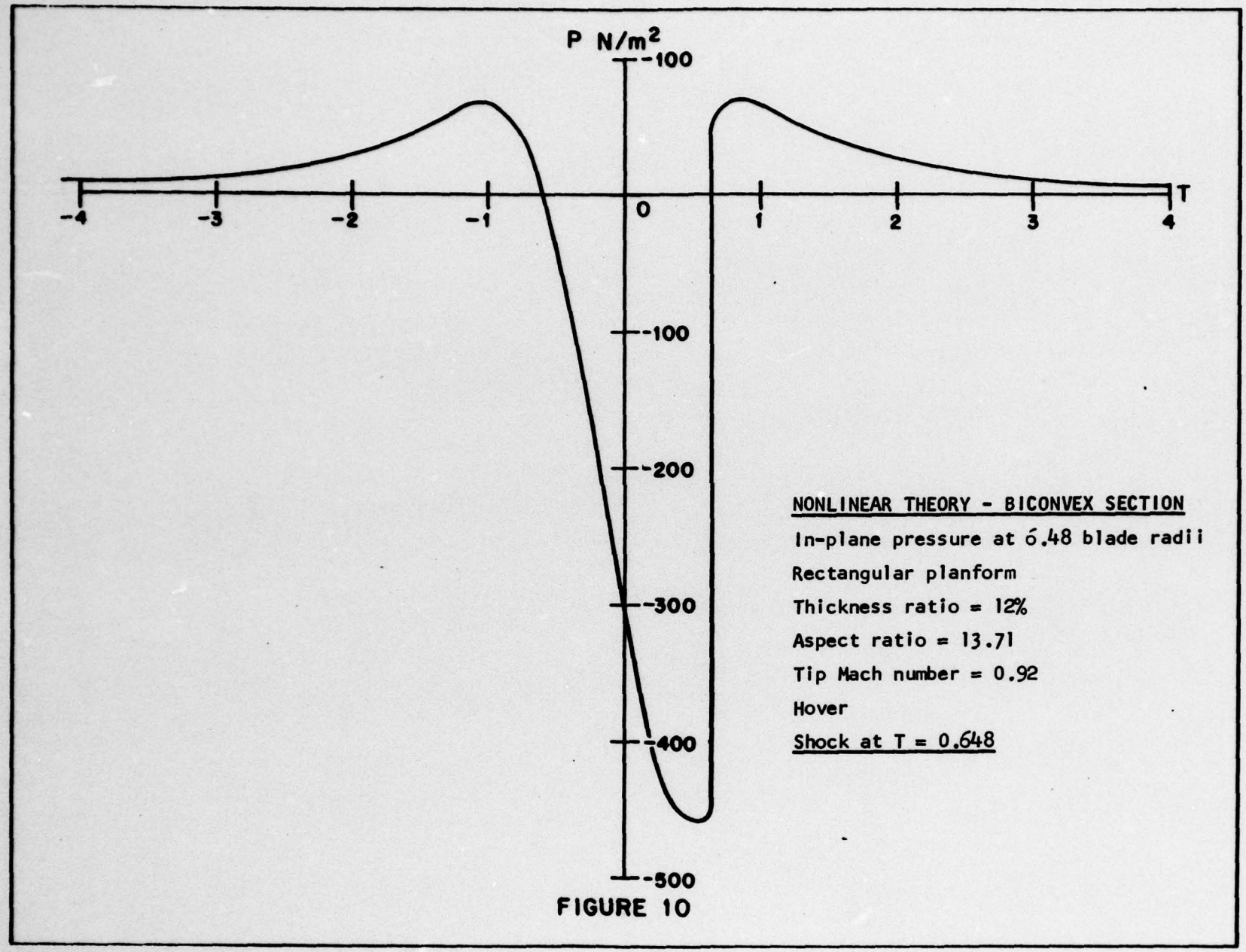
P N/m²
-100
-200
-300
-400
-500
-4
-3
-2
-1
0
1
2
3
4
T
NONLINEAR THEORY - BICONVEX SECTION
In-plane pressure at ó.48 blade radii
Rectangular planform
Thickness ratio = 12%
Aspect ratio = 13.71
Tip Mach number = 0.92
Hover
Shock at T = 0.648

FIGURE 10

REFERENCES

1. Farassat, F., Theory of noise generation from moving bodies with an application to helicopter rotors. NASA TR R-451, December 1975.

2. Hawkings, D. L., and M. V. Lowson, Theory of open supersonic rotor noise. Journal of Sound and Vibration, Vol. 36, No. 1, 1974.

3. Schmitz, F. H., and Y. H. Yu, Theoretical modeling of high-speed helicopter impulsive noise. Third European Rotorcraft and Powered Lift Aircraft Forum, Paper No. 54, Aix-en-Provence, France, September 7-9, 1977.

4. Vause, C. R., F. H. Schmitz, and D. A. Boxwell, 32nd Annual National V/STOL Forum of the American Helicopter Society, Washington, D. C., May 1976.

5. Boxwell, D. A., Y. H. Yu, and F. H. Schmitz, Hovering impulsive noise — some measured and calculated results. AHS-NASA-Army Acoustic Symposium, Langley Research Center, May 1978.

6. Caradonna, Francis X., and Morris P. Isom, Subsonic and transonic potential flow over helicopter rotor blades. AIAA Journal, Vol. 10, No. 12, December 1972.

7. Caradonna, F. X., and M. P. Isom, Numerical calculation of unsteady transonic potential flow over helicopter rotor blades. AIAA Journal, Vol. 14, No. 4, April 1976.

8. Yu, Yung H., Frank X. Caradonna, and Fredric H. Schmitz, The influence of the transonic flow field on high-speed helicopter impulsive noise. Fourth European Rotorcraft and Powered Lift Aircraft Forum. Stresa, Italy, September 13-15, 1978.

9. Whitham, G. B., Linear and Nonlinear Waves, John Wiley and Sons, New York, 1974.

10. Ffowcs Williams, J. E., and D. L. Hawkings, Sound generation by turbulance and surfaces in arbitrary motion. Philosophical Transactions of the Royal Society of London, Series A, Vol. 264, May 8, 1969.

11. Isom, M. P., The theory of sound radiated by a hovering transonic helicopter blade. Poly-AE/AM Report No. 75-4, Department of Aerospace Engineering and Applied Mechanics, Polytechnic Institute of New York, May 1975.